

# Multilevel neural simulation-based inference

Yuga Hikida\* Ayush Bharti\* Niall Jeffrey† François-Xavier Briol‡

## Abstract

Neural simulation-based inference (SBI) is a popular set of methods for Bayesian inference when models are only available in the form of a simulator. These methods are widely used in the sciences and engineering, where writing down a likelihood can be significantly more challenging than constructing a simulator. However, the performance of neural SBI can suffer when simulators are computationally expensive, thereby limiting the number of simulations that can be performed. In this paper, we propose a novel approach to neural SBI which leverages multilevel Monte Carlo techniques for settings where several simulators of varying cost and fidelity are available. We demonstrate through both theoretical analysis and extensive experiments that our method can significantly enhance the accuracy of SBI methods given a fixed computational budget.

## 1 Introduction

Simulation-based inference (SBI) (Cranmer et al., 2020) is a set of methods used to estimate parameters of complex models for which the likelihood is intractable but simulating data is possible. It is particularly useful in fields such as cosmology (Jeffrey et al., 2021), epidemiology (Kypriaios et al., 2017), ecology (Beaumont, 2010), synthetic biology (Lintusaari et al., 2017), and telecommunications engineering (Bharti et al., 2022a), where models describe intricate physical or biological processes such as galaxy formation, spread of diseases, the interaction of cells, or propagation of radio signals.

For a long time, SBI was dominated by methods such as approximate Bayesian computation (ABC) (Beaumont et al., 2002; Beaumont, 2019), which compared summary statistics of simulations and of the observed data. However, SBI methods using neural networks to approximate likelihoods (Papamakarios et al., 2019; Lueckmann et al., 2019; Boelts et al., 2022), likelihood ratios (Thomas et al., 2022; Durkan et al., 2020; Hermans et al., 2020), or posterior distributions (Papamakarios and Murray, 2016; Lueckmann et al., 2017; Greenberg et al., 2019; Radev et al., 2022) are now quickly becoming the preferred approach. These *neural SBI* methods are often favoured because they allow for amortisation (Zammit-Mangion et al., 2024), meaning that they require a large offline cost to train the neural network, but once the network is trained, the method can rapidly infer parameters for new observations or different priors without requiring additional costly simulations. This is particularly useful when the simulator is computationally expensive, as it reduces the need to repeatedly run simulations for each new inference task, making the overall process significantly less costly.

---

\*Department of Computer Science, Aalto University, Finland. Email: {yuga.hikida, ayush.bharti}@aalto.fi

†Department of Physics & Astronomy, University College London, UK. Email: n.jeffrey@ucl.ac.uk

‡Department of Statistical Science, University College London, London, UK. Email: f.briol@ucl.ac.uk

Nevertheless, the initial training phase of neural SBI methods typically still requires a large number of simulations, preventing their application on more computationally expensive (and often more realistic) models which can take hours of compute time for simulating a single data-point. Examples include most tsunami models (Behrens and Dias, 2015), wind farm models (Kirby et al., 2023), nuclear fusion (Hoppe et al., 2021) and cosmology (Jeffrey et al., 2025) simulators. One potential approach to mitigating this issue is multi-fidelity methods (Peherstorfer et al., 2018): instead of relying on a single simulator, we often have access to a sequence of simulators with increasing computational cost and accuracy which we may be able to use to refine existing methods. This setting is quite common; for instance, for simulators requiring the numerical solution of ordinary, partial, or stochastic differential equations, where the choice of mesh size or step-size affects both the accuracy of the solution and the computational cost. Another example arises when modelling complex physical, chemical, or biological processes, where simplified approximations can be obtained by neglecting certain aspects of the system. This is exemplified in Figure 1, where a high-fidelity cosmological simulation includes baryonic astrophysics and thus appear smoother than the low-fidelity simulation.

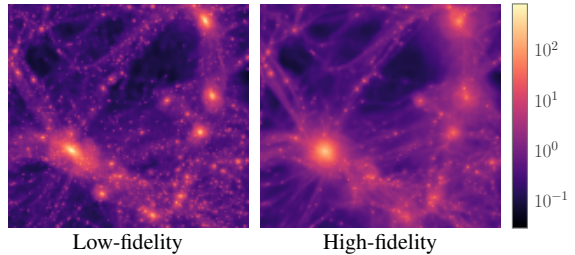


Figure 1: Low- and high-fidelity cosmological simulations from the CAMELS data (Villaescusa-Navarro et al., 2023) studied in Section 5.4.

The key idea behind multi-fidelity methods is to leverage cheaper, less accurate simulations to supplement the more expensive, high-fidelity simulations, ultimately improving efficiency without sacrificing accuracy. This has been popular in the emulation literature since the seminal work of Kennedy and O’Hagan (2000), but applications to SBI are much more recent and include Jasra et al. (2019); Warne et al. (2018); Prescott and Baker (2020, 2021); Warne et al. (2022); Prescott et al. (2024), who proposed multi-fidelity versions of ABC. More recently, (Krouglova et al., 2025) also proposed a multi-fidelity method to enhance neural SBI approximations of the posterior based on transfer learning. However, their method is not supported by any theoretical guarantees, and our numerical experiments in Section 5.2 will demonstrate that it is sensitive to choices of hyperparameters and the paper does not provide any guidance for selecting these.

In this paper, we propose a novel multi-fidelity method which is broadly applicable to neural SBI methods. Taking neural likelihood and neural posterior estimation as the main case-studies, we show that our approach is able to significantly reduce the computational cost of the initial training through the use of multilevel Monte Carlo (Giles, 2015; Jasra et al., 2020) estimates of the training objective. The approach has strong theoretical guarantees; under mild conditions, our main result (Theorem 1) directly links the reduction in computational cost to the accuracy of the low fidelity simulators, and we demonstrate (in Theorem 2) how to best balance the number of simulations at each fidelity level in the process. Importantly, and unlike Krouglova et al. (2025), our method has no additional hyperparameter. Our extensive experiments on models from finance, synthetic biology, and cosmology also demonstrate the significant computational advantages provided by our method.

## 2 Background

We first recall the basics of SBI methods and the related works on reducing computational cost in Section 2.1, then provide a brief introduction to multilevel Monte Carlo in Section 2.2.

### 2.1 Simulation-based inference

Let  $\{\mathbb{P}_\theta : \theta \in \Theta\}$  be a parametric model family of distributions on some space  $\mathcal{X} \subseteq \mathbb{R}^{d_{\mathcal{X}}}$  parameterised by  $\theta \in \Theta \subseteq \mathbb{R}^{d_\Theta}$ . We assume that the model is available in the form of a computer code, i.e. as a *simulator*, wherein simulating realisations  $x \sim \mathbb{P}_\theta$  is straightforward, but the likelihood function  $p(\cdot | \theta)$  associated with  $\mathbb{P}_\theta$  is intractable. The generative process of simulators can be characterised by a pair  $(\mathbb{U}, G_\theta)$ , where  $\mathbb{U}$  is a distribution (typically simple, such as a uniform or a Gaussian) on a space  $\mathcal{U} \subseteq \mathbb{R}^{d_{\mathcal{U}}}$  which captures all of the randomness, and  $G_\theta : \mathcal{U} \mapsto \mathcal{X}$  is a (deterministic) parametric map called the *generator*. Sampling  $x \sim \mathbb{P}_\theta$  requires first sampling  $u \sim \mathbb{U}$ , and then applying the generator  $x = G_\theta(u)$ . In this paper, we consider the classical Bayesian inference problem of estimating the parameters  $\theta$  of this simulator-based model given independent and identically distributed (iid) data  $x_{1:m}^o = \{x_j^o\}_{j=1}^m \in \mathcal{X}^m$  collected from some true data-generating process. Specifically, we are interested in estimating the posterior distribution  $\pi(\theta | x_{1:m}^o) \propto \prod_{j=1}^m p(x_j^o | \theta) \pi(\theta)$ , where  $\pi(\theta)$  is the prior distribution. As introduced below, this can for example be achieved via a neural SBI method which approximates the likelihood or posterior distribution.

**Neural likelihood estimation (NLE).** NLEs (Papamakarios et al., 2019; Lueckmann et al., 2019; Boelts et al., 2022; Radev et al., 2023a) are extensions of the synthetic likelihood approach (Wood, 2010; Price et al., 2018) that use flexible conditional density estimators, typically normalising flows (Rezende and Mohamed, 2015; Papamakarios et al., 2021), as surrogate models for the density of  $\mathbb{P}_\theta$ , i.e., the intractable likelihood function. The surrogate conditional density  $q_\phi^{\text{NLE}} : \mathcal{X} \times \Theta \rightarrow [0, \infty)$  where  $q_\phi^{\text{NLE}}(\cdot | \theta)$  is a density function for each  $\theta \in \Theta$  and  $\phi \in \Phi \subseteq \mathbb{R}^{d_\Phi}$  denotes its learnable parameters, is trained by minimising the negative log-likelihood with respect to  $\phi$  on simulated samples. More precisely, let  $\{(\theta_i, x_i)\}_{i=1}^n$  be the training data such that  $\theta_i \sim \pi$  are realisations from the prior and  $x_i \sim \mathbb{P}_{\theta_i}$  are realisations from the simulator, then  $\hat{\phi}_{\text{MC}} := \arg \min_{\phi \in \Phi} \ell_{\text{MC}}^{\text{NLE}}(\phi)$ , where  $\ell_{\text{MC}}^{\text{NLE}}$  is an empirical (Monte Carlo) estimate of negative expected log-density:

$$\ell^{\text{NLE}}(\phi) := -\mathbb{E}_{\theta \sim \pi} [\mathbb{E}_{x \sim \mathbb{P}_\theta} [\log q_\phi^{\text{NLE}}(x | \theta)]] \approx -\frac{1}{n} \sum_{i=1}^n \log q_\phi^{\text{NLE}}(x_i | \theta_i) =: \ell_{\text{MC}}^{\text{NLE}}(\phi).$$

Once the surrogate likelihood is trained, Markov chain Monte Carlo (MCMC) or variational inference methods are used to sample from the (approximate) posterior distribution  $\pi_{\text{NLE}}(\theta | x_{1:m}^o) \propto \prod_{j=1}^m q_{\hat{\phi}_{\text{MC}}}^{\text{NLE}}(x_j^o | \theta) \pi(\theta)$ . NLEs can therefore be regarded as being partially amortised—the surrogate  $q_\phi^{\text{NLE}}$  need not be trained for a new observed dataset, however, MCMC needs to be carried out again. For a computationally costly simulator, we note that obtaining training samples can become a bottleneck, which affects the accuracy of estimating the expected loss. Thus, estimating the loss accurately with fewer samples is key to handling costly simulators.

**Neural posterior estimation (NPE).** Instead of learning a surrogate likelihood, NPEs learn a mapping  $x \mapsto p(\theta | x)$  from the data to the posterior using conditional density estimators that are based on normalising flow (Papamakarios and Murray, 2016; Radev et al., 2022), diffusion (Geffner et al., 2023; Sharrock et al., 2024; Gloeckler et al., 2024), or consistency models (Schmitt et al., 2024b). Similar to NLE, the conditional density  $q_\phi^{\text{NPE}} : \Theta \times \mathcal{X}^m \rightarrow [0, \infty)$  is trained by minimising the negative log likelihood with respect to  $\phi$  using data  $\{(\theta_i, x_{1:m,i})\}_{i=1}^n$  generated by first sampling from the prior  $\theta_i \sim \pi$  and then the simulator  $x_{1:m,i} = (x_{1,i}, \dots, x_{m,i}) \sim \mathbb{P}_{\theta_i}$ :

$$\ell^{\text{NPE}}(\phi) := -\mathbb{E}_{\theta \sim \pi} [\mathbb{E}_{x_{1:m} \sim \mathbb{P}_\theta} [\log q_\phi^{\text{NPE}}(\theta | x_{1:m})]] \approx -\frac{1}{n} \sum_{i=1}^n \log q_\phi^{\text{NPE}}(\theta_i | x_{1:m,i}) =: \ell_{\text{MC}}^{\text{NPE}}(\phi)$$

Once  $\phi$  is estimated, the NPE posterior is obtained as  $\pi_{\text{NPE}}(\theta | x_{1:m}^o) = q_{\hat{\phi}_{\text{MC}}}^{\text{NPE}}(\theta | x_{1:m}^o)$ . Although training  $q_\phi^{\text{NPE}}$  incurs an upfront cost, this is a one-time cost as approximate posteriors for new observed datasets are obtained by a simple forward pass of  $x_{1:m}^o$  through the trained networks, making NPEs fully amortised. Similar to NLE, the computationally costly step in NPE is the generation of training samples from running expensive simulators.

Note that both  $q_\phi^{\text{NLE}}$  and  $q_\phi^{\text{NPE}}$  usually include a summary function (often architecturally implicit in NPE). This is helpful when  $\mathcal{X}$  is high-dimensional or the number of observations  $m$  is large (Alsing et al., 2018; Radev et al., 2022), and for NPE it allows conditioning on datasets of different sizes.

**Related work on reducing the cost of SBI methods.** We briefly note that beyond the aforementioned multi-fidelity methods, other works also aim to reduce the computational cost of SBI. In the context of ABC, adaptive sampling of the posterior using either sequential Monte Carlo techniques (Sisson et al., 2007; Beaumont et al., 2009; D. Moral et al., 2011) or Gaussian process surrogates (Gutmann and Corander, 2016; Meeds and Welling, 2014) has been a popular approach. A similar approach has been applied to neural SBI (Papamakarios and Murray, 2016; Lueckmann et al., 2017; Greenberg et al., 2019; Papamakarios et al., 2019; Hermans et al., 2020; Durkan et al., 2020), where sequential training schemes are employed to reduce the number of calls to the simulator. Other works have tackled this problem using cost-aware sampling (Bharti et al., 2025), side-stepping high-dimensional estimation (Jeffrey and Wandelt, 2020), early stopping of simulations (Prangle, 2016), dependent simulations (Niu et al., 2023; Bharti et al., 2023), expert-in-the-loop methods (Bharti et al., 2022b), self-consistency properties (Schmitt et al., 2024a), parallelisation of computations (Kulkarni and Moritz, 2023), and the Markovian structure of certain simulators (Gloeckler et al., 2025). Our method, which employs multilevel Monte Carlo, can be combined with all of these compute-efficient SBI methods and is hence complementary to them.

## 2.2 Multilevel Monte Carlo method

Consider some square-integrable function  $f : \mathcal{Z} \rightarrow \mathbb{R}$  and distribution  $\mu$  on a domain  $\mathcal{Z} \subseteq \mathbb{R}^{dz}$ . We consider the task of estimating  $\mathbb{E}_{z \sim \mu}[f(z)]$ . A first approach is *standard Monte Carlo (MC)* (Robert and Casella, 2000; Owen, 2013), which yields the following estimator:  $1/n \sum_{i=1}^n f(z_i)$ , where  $z_1, \dots, z_n \sim \mu$ . The root-mean-squared error (RMSE) of this estimator converges at a rate  $O(n^{-1/2})$ , where the rate constant is controlled by  $\text{Var}[f(z)]$  (Owen, 2013,

Ch. 2). In cases where  $f$  is expensive to evaluate or  $\mu$  is expensive to sample from, the RMSE can therefore be relatively large.

This issue can be mitigated by *multilevel Monte Carlo (MLMC)*, which was first proposed by Heinrich (2001); Giles (2008), and more recently reviewed in Giles (2015); Jasra et al. (2020). Suppose we have a sequence of square-integrable functions  $f_l : \mathcal{Z} \rightarrow \mathbb{R}$  for  $l \in \{0, 1, \dots, L\}$  which are approximations of  $f$  and which are ordered such that  $f_L = f$ , and both the cost of evaluation  $C_l$  and the accuracy (or *fidelity*) of  $f_l$  increases with  $l$ . In that case, MLMC consists of expressing  $\mathbb{E}_{z \sim \mu}[f(z)]$  through a telescoping sum and approximating each term through MC based on samples  $z_i^l \sim \mu$  for  $i = 1, \dots, n_l$  and  $l = \{0, 1, \dots, L\}$ :

$$\begin{aligned} \mathbb{E}_{z \sim \mu}[f(z)] &= \mathbb{E}_{z \sim \mu}[f_0(z)] + \sum_{l=1}^L \mathbb{E}_{z \sim \mu}[f_l(z) - f_{l-1}(z)] \\ &\approx \frac{1}{n_0} \sum_{i=1}^{n_0} f_0(z_i^0) + \sum_{l=1}^L \left( \frac{1}{n_l} \sum_{i=1}^{n_l} (f_l(z_i^l) - f_{l-1}(z_i^l)) \right) \end{aligned}$$

Note that this can also be thought of as using the low-fidelity functions as approximate control variates. By carefully balancing the number of samples  $n_0, \dots, n_L$  according to the costs  $C_0, \dots, C_L$  and variances  $\text{Var}[f_0(z)], \text{Var}[f_1(z) - f_0(z)], \dots, \text{Var}[f_L(z) - f_{L-1}(z)]$  at each level, one can show that MLMC can significantly improve on the accuracy of MC given a fixed computational budget. For this reason, MLMC has found numerous applications in statistics and machine learning, including for optimisation (Asi et al., 2021; Hu et al., 2023; Yang et al., 2024), sampling (Dodwell et al., 2019; Jasra et al., 2020), variational inference (Fujisawa and Sato, 2021; Shi and Cornish, 2021), probabilistic numerics (Li et al., 2023; Chen et al., 2025) and the design of experiments (Goda et al., 2020, 2022).

### 3 Methodology

We now present NLE and NPE versions of our approach, termed *multilevel-NLE* and *multilevel-NPE*.

**MLMC for NLE and NPE.** Recall that we are performing inference for a simulator  $(G_\theta, \mathbb{U})$  with a prior  $\pi$  on the parameter  $\theta \in \Theta$ . We reparameterise the NLE and the NPE objective in terms of  $u$  instead of  $x$  (akin to the reparametrisation trick in variational inference), and express them more broadly using an arbitrary loss  $\ell$  (to represent either  $\ell^{\text{NLE}}$  or  $\ell^{\text{NPE}}$ ) and an arbitrary function  $f_\phi$  (to represent either  $f_\phi^{\text{NLE}}$  or  $f_\phi^{\text{NPE}}$ ) as:

$$\ell(\phi) := \mathbb{E}_{\theta \sim \pi, u_{1:m} \sim \mathbb{U}} [f_\phi(u_{1:m}, \theta)],$$

where for NLE we have  $f_\phi^{\text{NLE}}(u, \theta) := -\log q_\phi^{\text{NLE}}(G_\theta(u)|\theta) = -\log q_\phi^{\text{NLE}}(x|\theta)$  with  $m = 1$ , and for NPE we have  $f_\phi^{\text{NPE}}(u_{1:m}, \theta) := -\log q_\phi^{\text{NPE}}(\theta | G_\theta(u_1), \dots, G_\theta(u_m)) = -\log q_\phi^{\text{NPE}}(\theta | x_{1:m})$ . Hereafter, we present our methods using  $f_\phi$  and  $\ell$  in order to avoid duplication.

The MC estimator of the loss  $\ell(\phi)$  is given by  $\ell_{\text{MC}}(\phi) := \frac{1}{n} \sum_{i=1}^n f_\phi(u_{1:m,i}, \theta_i)$ . Note that the variance of this MC estimator depends on the number of iid samples  $n$ . Hence, a small  $n$  owing to a computationally expensive simulator will lead to a poor estimator for the loss. Now suppose that we have access to a sequence simulators (or generators)

$G_\theta^0(u), \dots, G_\theta^{L-1}(u)$  with varying fidelity levels. Then, for  $l = 0, \dots, L-1$ , we can define a corresponding sequence of functions  $f_\phi^l(u_{1:m}, \theta)$ :

$$f_\phi^{\text{NLE},l}(u_{1:m}, \theta) := -\log q_\phi^{\text{NLE}}\left(G_\theta^l(u) \mid \theta\right), \text{ and } f_\phi^{\text{NPE},l}(u_{1:m}, \theta) := -\log q_\phi^{\text{NPE}}\left(\theta \mid G_\theta^l(u_1), \dots, G_\theta^l(u_m)\right),$$

such that  $f_\phi^L(u_{1:m}, \theta) := f_\phi(u_{1:m}, \theta)$ . This sequence of functions gives evaluations of the log conditional density at evaluations of the (approximate) simulator. Recall that the larger the value of  $l$ , the more accurate (and computationally expensive) such simulations will tend to be. At this point, we can re-express the objective using a telescoping sum as

$$\begin{aligned} \ell(\phi) &:= \mathbb{E}_{\theta \sim \pi, u_{1:m} \sim \mathbb{U}} [f_\phi(u_{1:m}, \theta)] = \mathbb{E}_{\theta \sim \pi, u_{1:m} \sim \mathbb{U}} \left[ f_\phi^L(u_{1:m}, \theta) \right] \\ &= \mathbb{E}_{\theta \sim \pi, u_{1:m} \sim \mathbb{U}} \left[ f_\phi^0(u_{1:m}, \theta) \right] + \sum_{l=1}^L \mathbb{E}_{\theta \sim \pi, u_{1:m} \sim \mathbb{U}} \left[ f_\phi^l(u_{1:m}, \theta) - f_\phi^{l-1}(u_{1:m}, \theta) \right]. \end{aligned} \quad (1)$$

Equation (1) follows by adding then subtracting some terms, and using linearity of expectations. Now suppose that we can simulate from each of these approximate simulators to obtain:

$$\left\{ \theta_i^l, u_{1:m,i}^l, G_{\theta_i^l}^l(u_{1,i}^l), \dots, G_{\theta_i^l}^{l-1}(u_{m,i}^l) \right\} \quad \text{where } \theta_i^l \sim \pi, u_{1:m,i}^l \sim \mathbb{U},$$

for  $i = 1, \dots, n_l$  and  $l = 0, \dots, L$ . We can then use these simulations to approximate each term in the telescoping sum through a Monte Carlo estimator as follows:

$$\ell(\phi) \approx \ell_{\text{MLMC}}(\phi) := \underbrace{\frac{1}{n_0} \sum_{i=1}^{n_0} f_\phi^0(u_{1:m,i}^0, \theta_i^0)}_{h_0(\phi)} + \sum_{l=1}^L \underbrace{\frac{1}{n_l} \sum_{i=1}^{n_l} \left( f_\phi^l(u_{1:m,i}^l, \theta_i^l) - f_\phi^{l-1}(u_{1:m,i}^l, \theta_i^l) \right)}_{h_l(\phi)} \quad (2)$$

This corresponds to an MLMC estimator of our original objective in (1). The idea is that  $h_0(\phi)$  is a cheap but rough estimate of  $\ell_{\text{MC}}(\phi)$ , and each additional term  $h_l(\phi)$  accounts for the difference between the  $l^{\text{th}}$  and the  $(l-1)^{\text{th}}$  level. Thus, the sum  $\sum_{l=1}^L h_l(\phi)$  ‘‘corrects’’ for the difference between  $\ell_{\text{MC}}(\phi)$  (which is based on high-fidelity simulations) and  $h_0(\phi)$  (which is based on low-fidelity simulations). Note that  $f_\phi^l$  and  $f_\phi^{l-1}$  share the same random samples  $u_{1:m}^l$ , i.e., they are seed matched. This ensures that  $f_\phi^l$  and  $f_\phi^{l-1}$  are coupled and highly correlated, leading to a reduction in the variance of  $h_l(\phi)$  term (Owen, 2013, Ch. 8).

**Computational cost.** Let  $C_l$  be the computational cost of sampling one  $x$  from the  $l^{\text{th}}$  level generator  $G_\theta^l$  and evaluating  $f_\phi^l$ , and recall that  $C_0 < C_1 < \dots < C_L$ . Then, the cost of MLMC is

$$\text{Cost}(\ell_{\text{MLMC}}(\phi); n_0, \dots, n_L) = \mathcal{O} \left( n_0 C_0 + \sum_{l=1}^L n_l (C_l + C_{l-1}) \right),$$

while that of the MC estimator is  $\text{Cost}(\ell_{\text{MC}}(\phi); n) = \mathcal{O}(n C_L)$ . Using solely the high-fidelity generator (as is customary in SBI) would require a large  $n$  in order to reasonably estimate  $\theta$ , thus increasing the total cost. However, with multiple lower-fidelity generators available, we can have a different number of simulated samples per level (i.e. we can take  $n_0 \neq n_1 \neq \dots \neq n_L$ ), and can select  $n_0, \dots, n_L$  such that  $n_l < n_{l-1}$ . This allows us to take a much larger number of samples from the cheaper (or low  $C_l$ ) approximations of the simulator, and a much smaller number of samples from the expensive (or high  $C_l$ ) approximations of the simulator, making MLMC particularly attractive for reducing the total computational cost of simulation in neural SBI.

**Extensions.** There are several straightforward extensions of our approach which are not covered above so as to not overload notation, but which we now briefly mention. Firstly, each simulator could have its own base measure  $\mathbb{U}^l$ , which could be defined on spaces  $\{\mathcal{U}^l\}_{l=1}^L$  of different dimensions. This is not a problem since we could simply consider  $\mathbb{U}$  to be the tensor product measure and  $\mathcal{U}$  to be the corresponding tensor product space, in which case all equations above remain valid. However, to ensure the best possible performance, it will still be essential to seed match random numbers where there is overlap; see Owen (2013, Ch. 8) for more details on the use of common random numbers.

Secondly, although our discussion has pertained to multilevel-NLE and multilevel-NPE so far, it is straightforward to extend the MLMC approach to other neural SBI methods such as neural ratio estimation (Hermans et al., 2020; Durkan et al., 2020; Miller et al., 2022), score-based NPE (Geffner et al., 2023), flow-matching NPE (Wildberger et al., 2023), and GAN-based NPE (Ramesh et al., 2022) since these are all based on objectives which can be expressed as MC estimators.

**Optimisation of the MLMC objective.** Optimising the MLMC loss  $\ell_{\text{MLMC}}(\phi)$  in (2) can be challenging due to the conflicting terms  $\{\sum_{i=1}^{n_l} f_\phi^l(u_{1:m,i}^l, \theta_i^l), \sum_{i=1}^{n_{l+1}} -f_\phi^l(u_{1:m,i}^l, \theta_i^l)\}_{l=0}^{L-1}$ . These “positive” and “negative” terms approximate the same expectation  $\mathbb{E}[f_\phi^l]$ , but with opposite signs and different number of samples. Later on in the optimisation, as their gradients shrink, one of the terms typically begins to dominate, creating opposing gradient directions. This dynamic leads to unstable updates and, ultimately, causes divergence. To mitigate this issue, we aim for  $\nabla_\phi h_0(\phi)$  to provide a coarse approximation of  $\nabla_\phi \ell(\phi)$ , with the remaining levels serving as corrections. However, under naive optimisation, this breaks down due to imbalanced evolution of gradient throughout the training. To restore the balance, we first rescale the components of  $\{\nabla_\phi h_l(\phi)\}_{l=1}^L$  to enforce their corrective role, by making sure that the two opposing components within each  $\nabla_\phi h_l(\phi)$  have comparable norms so that their difference remains small and stable. Then, we apply the gradient surgery technique of Liu et al. (2020), projecting the gradients of  $h_0(\phi)$  and  $\sum_{l=1}^L h_l(\phi)$  onto each other’s normal planes to further facilitate the optimisation. A detailed explanation is provided in Appendix A.

## 4 Theory

We now present our main theoretical results. Theorem 1 expresses the variance of each of the terms in the telescoping sum approximation (see (2)) as a function of the number of simulations per level, and the magnitude of the difference in generators between consecutive levels. We say that  $\mu$  is log-concave if it has a density of the form  $\exp(-\psi(z))$  for some convex function  $\psi : \mathcal{Z} \rightarrow \mathbb{R}$ . We recall that for  $r \in [1, \infty]$ ,  $d, d' \in \mathbb{N}$  and a non-empty, open, connected set  $\mathcal{Z} \subseteq \mathbb{R}^d$ , the space of vector-valued  $r$ -integrable functions with respect to a probability distribution  $\mu$  is given by  $L^r(\mu) := \{g : \mathcal{Z} \rightarrow \mathbb{R}^{d'} : \|g\|_{L^r(\mu)} := (\int_{\mathcal{Z}} \|g(x)\|_2^r \mu(dx))^{1/r} < \infty\}$ . For  $\tau \in \mathbb{N}$ , the corresponding Sobolev space of vector-valued functions of smoothness  $\tau$  is given by  $W^{\tau,r}(\mu) := \{g : \mathcal{Z} \rightarrow \mathbb{R}^{d'} : \|g\|_{W^{\tau,r}(\mu)} = (\sum_{|\alpha| \leq \tau} \|D^\alpha g\|_{L^r(\mu)}^r)^{1/r} < \infty\}$ , where for a multi-index  $\alpha \in \mathbb{N}^d$ ,  $D^\alpha$  is the weak derivative operator corresponding to  $\alpha$ . Finally, we recall that a function  $g$  is locally  $K_{\text{Lip}}$ -smooth if its gradient is locally Lipschitz continuous with Lipschitz constant  $K_{\text{Lip}} > 0$ ; i.e. for all  $z, z'$  in some open set of  $\mathcal{Z}$ , we have that

$$\|\nabla g(z) - \nabla g(z')\|_2 \leq K_{\text{Lip}} \|z - z'\|_2.$$

**Theorem 1.** Let  $\phi \in \Phi$  and suppose the following assumptions hold:

(A1) The prior  $\pi$  and the base measure  $\mathbb{U}$  are log-concave distributions.

(A2) The generators satisfy  $\|G^l\|_{W^{1,4}(\pi \times \mathbb{U}^m)} \leq S_l$  for  $l \in \{0, 1, \dots, L\}$ .

(A3) One of the following conditions holds:

- **NLE:**  $x, \theta \mapsto \log q_\phi^{\text{NLE}}(x|\theta)$  is locally  $K_{\text{Lip}}(\phi)$ -smooth and satisfies the growth condition  $\|\nabla_x \log q_\phi^{\text{NLE}}(x|\theta)\|_2 \leq K_{\text{grow}}(\phi)(\|(x, \theta)\|_2 + 1)$  for some  $K_{\text{Lip}}(\phi), K_{\text{grow}}(\phi) > 0$ .
- **NPE:**  $x_1, \dots, x_m, \theta \mapsto \log q_\phi^{\text{NPE}}(\theta|x_1, \dots, x_m)$  is locally  $K_{\text{Lip}}(\phi)$ -smooth and satisfies the growth condition  $\|\nabla_\theta \log q_\phi^{\text{NPE}}(\theta|x_1, \dots, x_m)\|_2 \leq K_{\text{grow}}(\phi)(\|(x_1, \dots, x_m, \theta)\|_2 + 1)$  for some  $K_{\text{Lip}}(\phi), K_{\text{grow}}(\phi) > 0$ .

Then, for  $l \in \{1, \dots, L\}$  and  $K_0(\phi), \dots, K_L(\phi) > 0$  independent of  $n_0, \dots, n_L$ , we have that:

$$\begin{aligned} \text{Var}[h_0(\phi)] &\leq \frac{K_0(\phi)}{n_0} \left( \|G^0\|_{W^{1,4}(\pi \times \mathbb{U}^m)}^4 + 1 \right), \\ \text{and } \text{Var}[h_l(\phi)] &\leq \frac{K_l(\phi)}{n_l} \left( \|G^l - G^{l-1}\|_{W^{1,4}(\pi \times \mathbb{U}^m)}^2 + 1 \right) \end{aligned}$$

See Appendix B.1 for the proof, and we emphasise that the variance is over both parameters  $\theta$  and noise  $u_{1:m}$ . (A1) requires log-concavity, which is a strong condition, but this is only required of the prior and the base measure. However, in SBI these tend to be simple distributions such as Gaussians or uniforms, which satisfy this assumption; see Saumard and Wellner (2014) for how to verify log-concavity in practice. (A2) is relatively mild: it asks that  $G^0, \dots, G^L$  have at least one derivative in  $\theta$  and  $u$ , and for these generators and their derivatives to have a fourth moment. This will hold when the simulators are used to define sufficiently well-behaved data-generating processes, but will be violated for sufficiently heavy-tailed distributions (e.g. the Cauchy). Finally, (A3) is mild; it holds when the gradient of the log conditional density estimator is Lipschitz continuous, which is for example the case when the conditional density is twice continuously differentiable and the Hessian is bounded (see e.g. Lemma 2.3 of Wright and Recht (2022)). It also holds for models such as mixtures of Gaussians, which are used in mixture density networks and for normalising flows with sufficiently regular transformations. The key implication of this result is a bound on the variance of our objective:

$$\begin{aligned} \text{Var}[\ell_{\text{MLMC}}(\phi)] &\leq \frac{K_0(\phi)}{n_0} \left( \|G^0\|_{W^{1,4}(\pi \times \mathbb{U}^m)}^4 + 1 \right) \\ &\quad + \sum_{l=1}^L \frac{K_l(\phi)}{n_l} \left( \|G^l - G^{l-1}\|_{W^{1,4}(\pi \times \mathbb{U}^m)}^2 + 1 \right) \end{aligned} \quad (3)$$

In order to make this bound small, we need to make each term small. Typically,  $\|G^0\|_{W^{1,4}(\pi \times \mathbb{U}^m)}$  will be large, but this will be counter-balanced by taking  $n_0$  to be large. For the higher-fidelity levels, the number of samples  $n_l$  will typically be smaller, but this will be counter-balanced by the fact that  $\|G^l - G^{l-1}\|_{W^{1,4}(\pi \times \mathbb{U}^m)}$  is small whenever  $G^{l-1}$  is a good approximation of  $G^l$ . As we now show, we can directly use this bound to get an indication of how to select  $n_0, \dots, n_L$ .

**Theorem 2.** *Suppose the assumptions of Theorem 1 hold. Then, the values of  $n_0, \dots, n_L$  which minimise the upper bound on  $\text{Var}[\ell_{MLMC}(\phi)]$  in (3) given a fixed computational budget; i.e. for  $\text{Cost}(\ell_{MLMC}(\phi); n_0, \dots, n_L) \leq C_{budget}$  for some  $C_{budget} > 0$  are given by*

$$n_0^* \propto \frac{C_{budget}}{\sqrt{C_0}} \sqrt{\|G^0\|_{W^{1,4}(\pi \times \mathbb{U}^m)}^4 + 1}, \quad n_l^* \propto \frac{C_{budget}}{\sqrt{C_l + C_{l+1}}} \sqrt{\|G^l - G^{l-1}\|_{W^{1,4}(\pi \times \mathbb{U}^m)}^2 + 1}.$$

See Appendix B.2 for the proof. The denominator in these expressions demonstrates that the more expensive the simulator is at level  $l$ , the smaller we should make the number of simulations at that level. We note that this result provides useful intuition on how to select the number of sample per level, but may be hard to use in practice since it requires quantities which are often unknown. For example, computing Sobolev norms can be challenging, and the results implicitly depends on  $\phi$  through the constants  $K_0(\phi), \dots, K_L(\phi)$  of Theorem 1 (which are unlikely to be tight). This is a common limitation of MLMC theory; see Section 2 and 3 of Giles (2015) for a discussion.

## 5 Numerical Experiments

We compare the performance of our multilevel version of NLE and NPE with the MLMC loss, termed ML-NLE and ML-NPE, respectively, against their standard counterpart with the MC loss. We use the `sbi` library (Tejero-Cantero et al., 2020) implementation for NLE and NPE, see Appendix C for the details. The code to reproduce our experiments is available at <https://github.com/yugahikida/multilevel-sbi>.

### 5.1 The g-and-k distribution: an illustrative example

We first consider the g-and-k distribution (Prangle, 2020) as an illustrative example. This is a very flexible univariate distribution that is defined via its quantile function and has four parameters, controlling the mean, variance, skewness, and kurtosis respectively, making it challenging for SBI methods. It does not typically have a low-fidelity simulator, so we construct one through a Taylor approximation of the quantile function, see Appendix C.1 for details. This makes it a slightly contrived example, but the fact that the g-and-k allows for an efficient approximation of the likelihood will make it particularly convenient to study the performance of NLE-based methods.

We fix the number of low-fidelity samples ( $n_0 = 10^4$  for ML-NLE and  $n_0 = 10^3$  for ML-NPE) and vary the number of high-fidelity samples  $n_1$  to assess the improvement in performance of our methods as  $n_1$  increases. For ML-NLE, we compute the Kullback-Leibler divergence (KLD) between the estimated conditional density and a numerical approximation of the likelihood. For ML-NPE, we use the negative log-posterior density (NLPD) of the true  $\theta$  under the estimated posterior density as the metric. The results in Figure 2a and 2b show that the multilevel versions of NLE and NPE perform better than their standard counterparts (with MC loss) using just a fraction of the high-fidelity samples. Unsurprisingly, the performance of MLE-NLE and ML-NPE improves as  $n_1$  increases.

In Figure 2c, we show an example of the NLE densities learned, with additional examples in Appendix C.1. Our ML-NLE method is able to approximate the almost exact g-and-k density the best. The coverage plot in Figure 2d shows that ML-NPE yields slightly

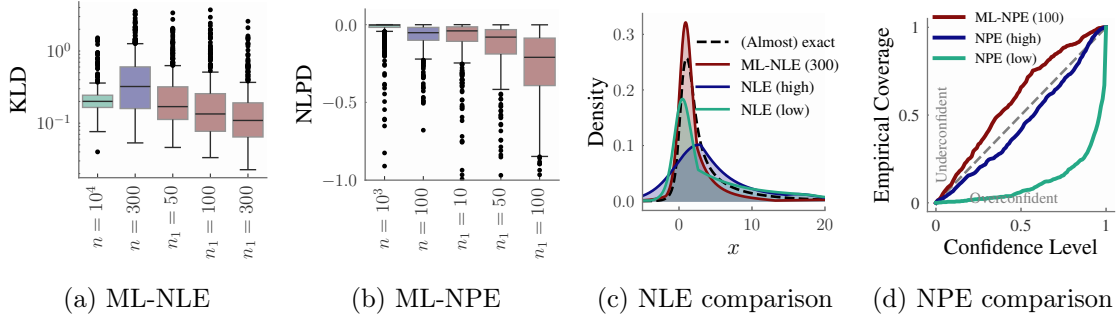


Figure 2: Performance of our **ML-NLE** and **ML-NPE** method on the g-and-k example. (a) KL-divergence ( $\downarrow$ ) between the estimated and the (almost) exact density for **ML-NLE** under different high-fidelity samples  $n_1$ . We compare it with **NLE (low)** trained on only low-fidelity data ( $n = 10^4$ ) and **NLE (high)**, trained on only high-fidelity data ( $n = 300$ ). (b) Negative log-posterior density (NLPD  $\downarrow$ ) for **ML-NPE**, **NPE (low)** with  $n = 10^3$ , and **NPE (high)** with  $n = 100$ . (c) One instance of learned densities using NLE. (d) Empirical coverage plot for **ML-NPE**, **NPE (low)**, and **NPE (high)**.

conservative posteriors as opposed to the overconfident posteriors obtained from NPE trained on either all low- or all high-fidelity data.

## 5.2 Ornstein–Uhlenbeck process: a popular financial model

Our next experiment involves the Ornstein-Uhlenbeck (OU) process—a stochastic differential equation model commonly used in financial analysis (Minenna, 2003), which in our case outputs a 100-dimensional Markovian time-series and has three parameters. The process is known to converge to a stationary Gaussian distribution, which we use as the low-fidelity simulator, see Appendix C.3. The example is reproduced from Krouglova et al. (2025), who used it for benchmarking their transfer learning approach to NPE (TL-NPE). TL-NPE first trains an NPE network on low-fidelity simulations, and then uses a small set of high-fidelity data to refine the network parameters until a stopping criterion is met. We implement TL-NPE with  $n_0 = 11,000$  and  $n_1 = 1000$ , using 10% of data as validation set for their stopping criterion, and compare against ML-NPE with  $n_0 = 10,000$  and  $n_1 = 1000$ . These values are picked so as to keep the simulation budget same for both the methods.

We compare ML-NPE with TL-NPE for different choices of its hyperparameter in Figure 3. TL-NPE’s hyperparameter is the number of epochs until the stopping criterion is activated, termed *patience*, which we let take values in  $\{1, 20, 10^2, 10^3\}$ . We use two metrics for evaluation: the NLPD of the true  $\theta$  under the estimated posterior, and the KLD between the posterior obtained using either TL-NPE or ML-NPE and a reference NPE posterior trained using  $n = 100,000$  samples. We observe that TL-NPE’s performance is quite sensitive to the choice of the patience value, and the authors of that work do not provide guidance on how to select this in practice (their code fixes this to 20 with no clear justification). When the number of high-fidelity samples are low ( $n_1 = 10$ ), its performance degrades as patience increases, as a higher patience means TL-NPE is overfitting to the few high-fidelity samples, losing the information gained from training on the low-fidelity data. In contrast, ML-NPE achieves better performance especially when  $n_1 = 10$  and does not have any hyperparameter to tune, making it easier to use in practice.

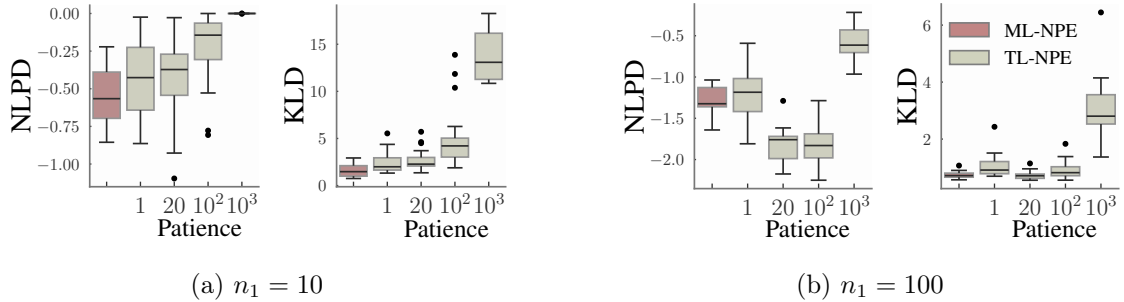


Figure 3: NLPD and KLD for **ML-NPE** (ours) and **TL-NPE** (Krouglova et al., 2025) using different patience values (hyperparameter of **TL-NPE**) over 20 runs. **ML-NPE** performs better in the limited high-fidelity data scenario ( $n_1 = 10$ ) (a), whilst being competitive when  $n_1 = 100$  (b). **TL-NPE** shows sensitivity towards its hyperparameter, while **ML-NPE** does not require any hyperparameter.

### 5.3 Toggle-switch model: a Systems Biology example

We now consider the toggle-switch model (Bonassi et al., 2011; Bonassi and West, 2015). This model describes the interaction between two genes over time, and has seven parameters and a scalar observation at the end of a time interval. Simulators typically use time-discretisation, and the total number of time-steps  $T$  acts as a fidelity parameter: running the model with large  $T$  incurs larger computational cost but leads to accurate simulations, while smaller  $T$  leads to cheap but inaccurate samples. Thus, this model illustrates a setting with more than two fidelity levels (by taking  $T$  to be more than two values)—a situation straightforward to handle with our multilevel approach but not with **TL-NPE** (Krouglova et al., 2025).

We take  $T_0 = 50$ ,  $T_1 = 80$ , and  $T_2 = 300$  to be the number of steps for the three fidelity levels, with  $n_0 = 10^4$ ,  $n_1 = 500$ , and  $n_2 = 300$ . Note that in this case each fidelity level has a different base measure of dimension  $2T + 1$ ; however, there is still sufficient seed-matching (see Appendix C.4 for details) and hence variance reduction thanks to MLMC. We compare our **ML-NLE** method with the standard **NLE** trained on samples from either the low- ( $n = 12,060$ ), the medium- ( $n = 7537$ ), or the high-fidelity simulator ( $n = 2010$ ). The number of training data  $n$  in each case is selected so as to match the total computational cost of simulation between **ML-NLE** and **NLE**, see Appendix C.4. Figure 4 reports the maximum mean discrepancy (MMD) (Gretton et al., 2012) between 500 samples from the learned conditional densities and 500 samples from the high-fidelity simulator across. We observe that **ML-NLE** performs better than all the **NLE** baselines for the same computational cost.

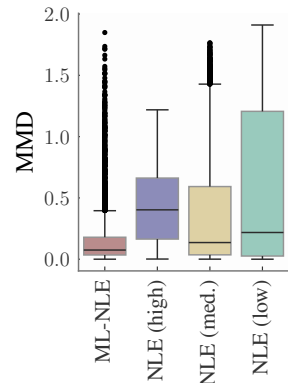


Figure 4: Boxplots of MMD ( $\downarrow$ ) across 5000 true parameter values for **NLE** and **ML-NLE**.

## 5.4 Cosmological Simulations

Finally, we consider a simulator from cosmology. We use the CAMELS simulation suite (Villaescusa-Navarro et al., 2021, 2023)—a benchmark dataset for machine learning in astrophysics—which comprises both low- and high-fidelity cosmological dataset. Our task is to infer a standard cosmological target parameter using a 39-dimensional power spectra of cosmology data, see Appendix C.5 for an example. The low-fidelity simulations are gravity-only N-body simulations, whose physical behaviour is controlled only by the parameter and some Gaussian fluctuations of the initial conditions. The high-fidelity hydrodynamic simulations have additional physics, controlled by an additional five parameters. We include these additional parameters as part of the  $\mathcal{U}$  space, constituting a case of partial common random numbers between the low- and high-fidelity simulators, similar to Section 5.3.

Here, the high-fidelity simulations can be orders of magnitude ( $> \times 100$ ) slower to generate than the low-fidelity ones, making this a representative problem for our method. Assuming we only have access to  $n = n_1 = 20$  high-fidelity simulations, we wish to ascertain the improvement in inference accuracy obtained by including 1000 low-fidelity simulations (i.e.  $n_0 = 980$ ) using our ML-NPE method. To that end, we measure the NLPD and empirical coverage of the estimated posteriors for 980 test data. The result in Figure 5 shows that ML-NPE performs better than standard NPE for both the metrics. Standard NPE tends to produce overconfident posteriors, while ML-NPE yields calibrated or underconfident posteriors for most confidence levels. Thus, including low-fidelity samples using our method leads to better inference.

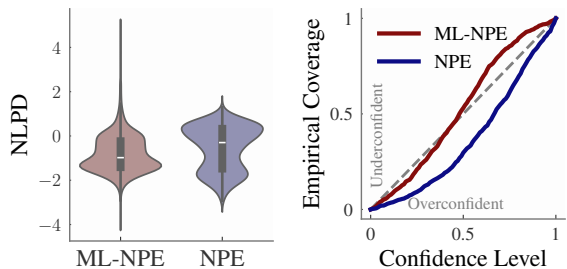


Figure 5: NLPD  $\downarrow$  and empirical coverage of NPE and ML-NPE for the cosmological inference task.

## 6 Conclusion

This paper shows how to reduce the cost of SBI using MLMC: by leveraging cheap low-fidelity simulations, our method performs accurate inference without requiring many samples from costlier simulators, which is the computational bottleneck in many applications. Moreover, our method does not have any hyperparameter to tune and it can handle more than two fidelity levels, unlike the method of Krouglova et al. (2025). More broadly, our method can be seen as a way to perform multilevel training of conditional density estimators in scenarios where data from different sources with different accuracy levels needs to be combined.

Our method is also particularly appealing since it is complementary to other compute-efficient SBI methods such as sequential SBI (Greenberg et al., 2019; Papamakarios et al., 2019), cost-aware SBI (Bharti et al., 2025), and NPE with self-consistency loss (Schmitt et al., 2024a), among others. A recent contemporary work (Tatsuoka et al., 2025) also proposed a two-step multi-fidelity SBI method, wherein an NPE network is first trained on low-fidelity data, and then the resulting posterior estimate is used to guide sampling from the high-fidelity simulator. This approach could easily be combined with our method by using MLMC to estimate the loss, making it complementary to us as well.

As our method involves gradient adjustments during optimisation, we observe a minor increase of roughly 15%-20% in training time compared to that of standard SBI methods, as reported in Appendix C.2. This however is not an issue as training time is usually negligible compared to running costly simulators, which is the setting we are in. Another limitation of the MLMC approach is that it is not applicable in cases where seed matching of the low- and high-fidelity simulators is not possible.

## Acknowledgments

The authors are grateful to Tim Sullivan for helpful discussions, and to the authors of Krouglova et al. (2025) for sharing their source code. YH and AB were supported by the Research Council of Finland grant no. 362534. FXB was supported by the EPSRC grant [EP/Y022300/1]. NJ was supported by the ERC-selected UKRI Frontier Research Grant EP/Y03015X/1 and by the Simons Collaboration on Learning the Universe.

## References

- J. Alsing, B. Wandelt, and S. Feeney. Massive optimal data compression and density estimation for scalable, likelihood-free inference in cosmology. *Monthly Notices of the Royal Astronomical Society*, 477(3):2874–2885, 2018. 4
- H. Asi, Y. Carmon, A. Jambulapati, Y. Jin, and A. Sidford. Stochastic bias-reduced gradient methods. In *Advances in Neural Information Processing Systems*, volume 34, pages 10810–10822, 2021. 5
- M. A. Beaumont. Approximate Bayesian computation in evolution and ecology. *Annual Review of Ecology, Evolution, and Systematics*, 41(1):379–406, 2010. 1
- M. A. Beaumont. Approximate Bayesian computation. *Annual Review of Statistics and Its Application*, 6(1):379–403, 2019. 1
- M. A. Beaumont, W. Zhang, and D. J. Balding. Approximate Bayesian computation in population genetics. *Genetics*, 162(4):2025–2035, 2002. 1
- M. A. Beaumont, J-M. Cornuet, J-M. Marin, and C. P. Robert. Adaptive approximate Bayesian computation. *Biometrika*, 96(4):983–990, 2009. 4
- J. Behrens and F. Dias. New computational methods in tsunami science. *Philosophical Transactions of the Royal Society A: Mathematical, Physical and Engineering Sciences*, 373(2053):20140382, 2015. 2
- A. Bharti, F-X. Briol, and T. Pedersen. A general method for calibrating stochastic radio channel models with kernels. *IEEE Transactions on Antennas and Propagation*, 70(6):3986–4001, 2022a. 1
- A. Bharti, L. Filstroff, and S. Kaski. Approximate Bayesian computation with domain expert in the loop. In *Proceedings of the 39th International Conference on Machine Learning*, volume 162, pages 1893–1905, 2022b. 4

- A. Bharti, M. Naslidnyk, O. Key, S. Kaski, and F-X. Briol. Optimally-weighted estimators of the maximum mean discrepancy for likelihood-free inference. In *Proceedings of the 40th International Conference on Machine Learning*, volume 202, pages 2289–2312, 2023. 4
- A. Bharti, D. Huang, S. Kaski, and F-X. Briol. Cost-aware simulation-based inference. In *Proceedings of The 28th International Conference on Artificial Intelligence and Statistics*, volume 258, pages 28–36, 2025. 4, 12
- C. M. Bishop. *Mixture density networks*. Aston University, 1994. 33
- S. G. Bobkov. Isoperimetric and analytic inequalities for log-concave probability measures. *The Annals of Probability*, 27(4):1903–1921, 1999. 22
- J. Boelts, J-M. Lueckmann, R. Gao, and J. H. Macke. Flexible and efficient simulation-based inference for models of decision-making. *Elife*, 11:e77220, 2022. 1, 3
- F. V. Bonassi and M. West. Sequential Monte Carlo with adaptive weights for approximate Bayesian computation. *Bayesian Analysis*, 10(1), 2015. 11
- F. V. Bonassi, L. You, and M. West. Bayesian learning from marginal data in bionetwork models. *Statistical applications in genetics and molecular biology*, 10(1), 2011. 11
- N. Chartier, B. Wandelt, Y. Akrami, and F. Villaescusa-Navarro. CARPool: Fast, accurate computation of large-scale structure statistics by pairing costly and cheap cosmological simulations. *Monthly Notices of the Royal Astronomical Society*, 503(2):1897–1914, 2021. ISSN 13652966. 34
- Nicolas Chartier and Benjamin D. Wandelt. CARPool covariance: Fast, unbiased covariance estimation for large-scale structure observables. *Monthly Notices of the Royal Astronomical Society*, 509(2):2220–2233, 2022. ISSN 13652966. doi: 10.1093/mnras/stab3097. 34
- Z. Chen, M. Naslidnyk, and F-X. Briol. Nested expectations with kernel quadrature. *arXiv:2502.18284*, 2025. 5
- K. Cranmer, J. Brehmer, and G. Louppe. The frontier of simulation-based inference. *Proceedings of the National Academy of Sciences*, 117(48):30055–30062, 2020. 1
- P. D. Moral, A. Doucet, and A. Jasra. An adaptive sequential Monte Carlo method for approximate Bayesian computation. *Statistics and Computing*, 22(5):1009–1020, 2011. 4
- T. J. Dodwell, C. Ketelsen, R. Scheichl, and A. L. Teckentrup. Multilevel Markov chain Monte Carlo. *SIAM Review*, 61(3):509–545, 2019. 5
- C. Durkan, A. Bekasov, I. Murray, and G. Papamakarios. Neural spline flows. In *Advances in Neural Information Processing Systems*, volume 32, pages 7511–7522, 2019. 29
- C. Durkan, I. Murray, and G. Papamakarios. On contrastive learning for likelihood-free inference. In *International Conference on Machine Learning*, volume 119, pages 2771–2781, 2020. 1, 4, 7
- M. Fujisawa and I. Sato. Multilevel Monte Carlo variational inference. *Journal of Machine Learning Research*, 22(278):1–44, 2021. 5

- M. Gatti et al. Dark Energy Survey Year 3 results: Simulation-based cosmological inference with wavelet harmonics, scattering transforms, and moments of weak lensing mass maps. II. cosmological results. *Physical Review D*, 111(6):063504, 2025. 34
- T. Geffner, G. Papamakarios, and A. Mnih. Compositional score modeling for simulation-based inference. In *Proceedings of the 40th International Conference on Machine Learning*, volume 202, pages 11098–11116, 2023. 4, 7
- M. B. Giles. Multilevel Monte Carlo path simulation. *Operations Research*, 56(3):607–617, 2008. 5
- M. B. Giles. Multilevel Monte Carlo methods. *Acta Numerica*, 24:259–328, 2015. 2, 5, 9
- M. Gloeckler, M. Deistler, C. D. Weilbach, F. Wood, and J. H. Macke. All-in-one simulation-based inference. In *Proceedings of the 41st International Conference on Machine Learning*, volume 235, pages 15735–15766, 2024. 4
- M. Gloeckler, S. Toyota, K. Fukumizu, and J. H. Macke. Compositional simulation-based inference for time series. In *The Thirteenth International Conference on Learning Representations*, 2025. 4
- T. Goda, T. Hironaka, and T. Iwamoto. Multilevel Monte Carlo estimation of expected information gains. *Stochastic Analysis and Applications*, 38(4):581–600, 2020. 5
- T. Goda, T. Hironaka, W. Kitade, and A. Foster. Unbiased MLMC stochastic gradient-based optimization of Bayesian experimental designs. *SIAM Journal on Scientific Computing*, 44(1):A286–A311, 2022. 5
- D. Greenberg, M. Nonnenmacher, and J. H. Macke. Automatic posterior transformation for likelihood-free inference. In *Proceedings of the 36th International Conference on Machine Learning*, pages 2404–2414, 2019. 1, 4, 12
- A. Gretton, K. Borgwardt, M. J. Rasch, and B. Scholkopf. A kernel two-sample test. *Journal of Machine Learning Research*, 13:723–773, 2012. 11
- M. U. Gutmann and J. Corander. Bayesian optimization for likelihood-free inference of simulator-based statistical models. *Journal of Machine Learning Research*, 17(125):1–47, 2016. 4
- S. Heinrich. Multilevel Monte Carlo methods. In *Large-Scale Scientific Computing*, volume 24, pages 58–67. Springer, 2001. 5
- J. Hermans, V. Begy, and G. Louppe. Likelihood-free MCMC with amortized approximate ratio estimators. In *Proceedings of the 37th International Conference on Machine Learning*, pages 4239–4248, 2020. 1, 4, 7
- M. Hoppe, O. Embreus, and T. Fülöp. Dream: A fluid-kinetic framework for tokamak disruption runaway electron simulations. *Computer Physics Communications*, 268:108098, 2021. 2
- Y. Hu, J. Wang, Y. Xie, A. Krause, and D. Kuhn. Contextual stochastic bilevel optimization. In *Thirty-seventh Conference on Neural Information Processing Systems*, 2023. 5

- A. Jasra, S. Jo, D. Nott, C. Shoemaker, and R. Tempone. Multilevel Monte Carlo in approximate Bayesian computation. *Stochastic Analysis and Applications*, 37(3):346–360, 2019. 2
- A. Jasra, K. Law, and C. Suci. Advanced Multilevel Monte Carlo Methods. *International Statistical Review*, 88(3):548–579, 2020. 2, 5
- N Jeffrey and B. D. Wandelt. Solving high-dimensional parameter inference: marginal posterior densities & Moment Networks. *Third Workshop on Machine Learning and the Physical Sciences, NeurIPS 2020*, art. arXiv:2011.05991, 2020. 4
- N. Jeffrey, J. Alsing, and F. Lanusse. Likelihood-free inference with neural compression of DES SV weak lensing map statistics. *Monthly Notices of the Royal Astronomical Society*, 501(1):954–969, 2021. 1
- N. Jeffrey et al. Dark energy survey year 3 results: likelihood-free, simulation-based  $\Lambda$ CDM inference with neural compression of weak-lensing map statistics. *Monthly Notices of the Royal Astronomical Society*, 536(2):1303–1322, 2025. 2, 34
- M. C. Kennedy and A. O’Hagan. Predicting the output from a complex computer code when fast approximations are available. *Biometrika*, 87:1–13, 2000. 2
- O. Key, A. Gretton, F.-X. Briol, and T. Fernandez. Composite goodness-of-fit tests with kernels. *Journal of Machine Learning Research*, 26(51):1–60, 2025. 32
- D. P. Kingma and J. Ba. Adam: A method for stochastic optimization. In *International Conference for Learning Representations*, 2015. 20, 28
- A. Kirby, F.-X. Briol, T. D. Dunstan, and T. Nishino. Data-driven modelling of turbine wake interactions and flow resistance in large wind farms. *Wind Energy*, 26(9):875–1011, 2023. 2
- A. N. Krouglova, H. R. Johnson, B. Confavreux, M. Deistler, and P. J. Gonçalves. Multifidelity simulation-based inference for computationally expensive simulators. *arXiv:2502.08416*, 2025. 2, 10, 11, 12, 13
- S. Kulkarni and C. A. Moritz. Improving effectiveness of simulation-based inference in the massively parallel regime. *IEEE Transactions on Parallel and Distributed Systems*, 34(4):1100–1114, 2023. 4
- T. Kypraios, P. Neal, and D. Prangle. A tutorial introduction to Bayesian inference for stochastic epidemic models using approximate Bayesian computation. *Mathematical Biosciences*, 287:42–53, 2017. 1
- K. Li, D. Giles, T. Karvonen, S. Guillas, and F.-X. Briol. Multilevel Bayesian quadrature. In *International Conference on Artificial Intelligence and Statistics*, pages 1845–1868, 2023. 5
- J. Lintusaari, M. U. Gutmann, R. Dutta, S. Kaski, and J. Corander. Fundamentals and recent developments in approximate Bayesian computation. *Systematic Biology*, 66:66–82, 2017. 1
- A. Liu, J. Z. Liu, J.-S. Denain, K. Gimpel, S. Sidor, S. Levine, and P. Abbeel. Gradient surgery for multi-task learning. In *Advances in Neural Information Processing Systems*, volume 33, pages 5824–5836, 2020. 7, 20

- J-M. Lueckmann, P. J. Gonçalves, G. Bassetto, K. Öcal, M. Nonnenmacher, and J. H. Macke. Flexible statistical inference for mechanistic models of neural dynamics. In *Advances in Neural Information Processing Systems*, page 1289–1299, 2017. 1, 4
- J-M. Lueckmann, G. Bassetto, T. Karaletsos, and J. H. Macke. Likelihood-free inference with emulator networks. In *Symposium on Advances in Approximate Bayesian Inference*, pages 32–53, 2019. 1, 3
- E. Meeds and M. Welling. GPS-ABC: Gaussian process surrogate approximate Bayesian computation. In *Proceedings of the Thirtieth Conference on Uncertainty in Artificial Intelligence*, page 593–602, 2014. 4
- B. K. Miller, C. Weniger, and P. Forré. Contrastive neural ratio estimation. In *Advances in Neural Information Processing Systems*, 2022. 7
- M. Minenna. The detection of market abuse on financial markets: A quantitative approach. *Quaderni di finanza*, 54, 2003. 10
- Z. Niu, J. Meier, and F-X Briol. Discrepancy-based inference for intractable generative models using quasi-Monte Carlo. *Electronic Journal of Statistics*, 17(1):1411–1456, 2023. 4
- A. B. Owen. *Monte Carlo theory, methods and examples*. <https://artowen.su.domains/mc/>, 2013. 4, 6, 7
- G. Papamakarios and I. Murray. Fast  $\epsilon$ -free inference of simulation models with Bayesian conditional density estimation. In *Advances in Neural Information Processing Systems*, pages 1036–1044, 2016. 1, 4
- G. Papamakarios, D. Sterratt, and I. Murray. Sequential neural likelihood: Fast likelihood-free inference with autoregressive flows. In *Proceedings of the Twenty-Second International Conference on Artificial Intelligence and Statistics*, pages 837–848, 2019. 1, 3, 4, 12
- G. Papamakarios, E. Nalisnick, S. Rezende, D. J. and Mohamed, and B. Lakshminarayanan. Normalizing flows for probabilistic modeling and inference. *Journal of Machine Learning Research*, 22(57):1–64, 2021. 3
- S. Paszke, A. and Gross, S. Chintala, E. Chanan, G. and Yang, Z. DeVito, Z. Lin, A. Desmaison, L. Antiga, and A. Lerer. Automatic differentiation in pytorch. In *NIPS-W*, 2017. 28
- B. Peherstorfer, K. Willcox, and M. Gunzburger. Survey of multifidelity methods in uncertainty propagation, inference, and optimization. *SIAM Review*, 60(3):550–591, 2018. 2
- D. Prangle. Lazy ABC. *Statistics and Computing*, 26:171–185, 2016. 4, 29
- D. Prangle. gk: An R Package for the g-and-k and Generalised g-and-h Distributions. *The R Journal*, 12(1):7, 2020. 9
- T. P. Prescott and R. E. Baker. Multifidelity approximate Bayesian computation. *SIAM-ASA Journal on Uncertainty Quantification*, 8(1):114–138, 2020. 2
- T. P. Prescott and R. E. Baker. Multifidelity approximate Bayesian computation with sequential Monte Carlo parameter sampling. *SIAM-ASA Journal on Uncertainty Quantification*, 9(2):788–817, 2021. 2

- T. P. Prescott, D. J. Warne, and R. E. Baker. Efficient multifidelity likelihood-free Bayesian inference with adaptive computational resource allocation. *Journal of Computational Physics*, 496:112577, 2024. 2
- W. H. Press. *Numerical recipes 3rd edition: The art of scientific computing*. Cambridge university press, 2007. 29
- L. F. Price, C. C. Drovandi, A. Lee, and D. J. Nott. Bayesian synthetic likelihood. *Journal of Computational and Graphical Statistics*, 27(1):1–11, 2018. 3
- S. T. Radev, U. K. Mertens, A. Voss, L. Ardizzone, and U. Köthe. Bayesflow: Learning complex stochastic models with invertible neural networks. *IEEE Transactions on Neural Networks and Learning Systems*, 33(4):1452–1466, 2022. 1, 4
- S. T. Radev, M. Schmitt, V. Pratz, U. Picchini, U. Köthe, and P-C. Bürkner. Jana: Jointly amortized neural approximation of complex bayesian models. In *Uncertainty in Artificial Intelligence*, pages 1695–1706, 2023a. 3
- S. T. Radev, M. Schmitt, L. Schumacher, L. Else Müller, V. Pratz, Y. Schälte, U. Köthe, and P-C. Bürkner. Bayesflow: Amortized bayesian workflows with neural networks. *Journal of Open Source Software*, 8(89):5702, 2023b. 28
- P. Ramesh, J-M. Lueckmann, J. Boelts, Á. Tejero-Cantero, D. S. Greenberg, P. J. Goncalves, and J. H. Macke. GATSBI: Generative adversarial training for simulation-based inference. In *International Conference on Learning Representations*, 2022. 7
- G. D. Rayner and H. L. MacGillivray. Numerical maximum likelihood estimation for the g-and-k and generalized g-and-h distributions. *Statistics and Computing*, 12(1):57–75, 2002. 29
- D. Rezende and S. Mohamed. Variational inference with normalizing flows. In *International conference on machine learning*, pages 1530–1538, 2015. 3
- C. P. Robert and G. Casella. *Monte Carlo Statistical Methods*. Springer, 2000. 4
- A. Saumard and J. A. Wellner. Log-concavity and strong log-concavity: A review. *Statistics Surveys*, 8:45–114, 2014. 8, 23, 24
- M. Schmitt, D. R. Ivanova, D. Habermann, U. Köthe, P-C. Bürkner, and S. T. Radev. Leveraging self-consistency for data-efficient amortized Bayesian inference. In *Proceedings of the 41st International Conference on Machine Learning*, 2024a. 4, 12
- M. Schmitt, V. Pratz, U. Köthe, P-C. Bürkner, and S. Radev. Consistency models for scalable and fast simulation-based inference. *Advances in Neural Information Processing Systems*, 37:126908–126945, 2024b. 4
- L. Sharrock, J. Simons, S. Liu, and M. Beaumont. Sequential neural score estimation: Likelihood-free inference with conditional score based diffusion models. In *Proceedings of the 41st International Conference on Machine Learning*, volume 235, pages 44565–44602, 2024. 4
- Y. Shi and R. Cornish. On multilevel monte carlo unbiased gradient estimation for deep latent variable models. In *Proceedings of The 24th International Conference on Artificial Intelligence and Statistics*, volume 130, pages 3925–3933, 2021. 5

- S. A. Sisson, Y. Fan, and Mark M. Tanaka. Sequential Monte Carlo without likelihoods. *Proceedings of the National Academy of Sciences*, 104(6):1760–1765, 2007. 4
- C. Tatsuoka, M. Yang, D. Xiu, and G. Zhang. Multi-fidelity parameter estimation using conditional diffusion models. *arXiv:2504.01894*, 2025. 12
- A. Tejero-Cantero, J. Boelts, M. Deistler, J-M. Lueckmann, C. Durkan, P. J. Gonçalves, D. S. Greenberg, and J. H. Macke. sbi: A toolkit for simulation-based inference. *Journal of Open Source Software*, 5(52):2505, 2020. 9, 28
- O. Thomas, R. Dutta, J. Corander, S. Kaski, and M. U. Gutmann. Likelihood-free inference by ratio estimation. *Bayesian Analysis*, 17(1):1–31, 2022. 1
- F. Villaescusa-Navarro et al. The CAMELS Project: Cosmology and Astrophysics with Machine-learning Simulations. *The Astrophysical Journal*, 915(1):71, 2021. 12, 34
- F. Villaescusa-Navarro et al. The CAMELS Project: Public Data Release. *The Astrophysical Journal Supplement Series*, 265(2):54, 2023. 2, 12, 34
- P. Virtanen et al. SciPy 1.0: Fundamental Algorithms for Scientific Computing in Python. *Nature Methods*, 17:261–272, 2020. 29
- D. J. Warne, R. E. Baker, and M. J. Simpson. Multilevel rejection sampling for approximate bayesian computation. *Computational Statistics & Data Analysis*, 124:71–86, 2018. 2
- D. J. Warne, T. P. Prescott, R. E. Baker, and M. J. Simpson. Multifidelity multilevel Monte Carlo to accelerate approximate Bayesian parameter inference for partially observed stochastic processes. *Journal of Computational Physics*, 469:111543, 2022. 2
- J. B. Wildberger, M. Dax, S. Buchholz, S. R. Green, J. H. Macke, and B. Schölkopf. Flow matching for scalable simulation-based inference. In *Thirty-seventh Conference on Neural Information Processing Systems*, 2023. 7
- S. N. Wood. Statistical inference for noisy nonlinear ecological dynamic systems. *Nature*, 466(7310):1102–1104, 2010. 3
- S. J. Wright and B. Recht. *Optimization for Data Analysis*. Cambridge University Press, 2022. 8
- S. Yang, V. Zankin, M. Balandat, S. Scherer, K. Carlberg, N. Walton, and K. J. H. Law. Accelerating look-ahead in Bayesian optimization: Multilevel Monte Carlo is all you need. In *International Conference on Machine Learning*, pages 56722–56748, 2024. 5
- A. Zammit-Mangion, M. Sainsbury-Dale, and R. Huser. Neural methods for amortized inference. *Annual Review of Statistics and Its Application*, 2024. 1

## Supplemental Material

The appendix is arranged as follows: In Appendix A, we discuss the implementation of the optimiser for our MLMC loss function. Appendix B contains the proofs of the theoretical results presented in Section 4. Lastly, Appendix C consists of the experimental details and additional results.

### A Optimising the MLMC objective

We can rewrite the objective in (2) as

$$\begin{aligned} \ell_{\text{MLMC}}(\phi) &= \frac{1}{n_0} \sum_{i=1}^{n_0} f_{\phi}^0(u_{1:m,i}^0, \theta_i^0) + \sum_{l=1}^L \frac{1}{n_l} \sum_{i=1}^{n_l} f_{\phi}^l(u_{1:m,i}^l, \theta_i^l) + \sum_{l=0}^{L-1} \frac{1}{n_{l+1}} \sum_{i=1}^{n_l} -f_{\phi}^l(u_{1:m,i}^l, \theta_i^l) \\ &:= \sum_{l=0}^L \bar{f}_{\phi}^{l,+} + \sum_{l=0}^{L-1} \bar{f}_{\phi}^{l,-} \end{aligned} \quad (4)$$

where  $\bar{f}_{\phi}^{l,+} := \frac{1}{n_l} \sum_{i=1}^{n_l} f_{\phi}^l(u_{1:m,i}^l, \theta_i^l)$  and  $\bar{f}_{\phi}^{l,-} := \frac{1}{n_{l+1}} \sum_{i=1}^{n_{l+1}} -f_{\phi}^l(u_{1:m,i}^l, \theta_i^l)$ . Since  $\bar{f}_{\phi}^{l,+}$  and  $\bar{f}_{\phi}^{l,-}$  are MC estimates of  $\mathbb{E}[f_{\phi}^l]$  and  $-\mathbb{E}[f_{\phi}^l]$  respectively with different number of samples, the loss function involves  $L - 1$  conflicting objectives.

When applying standard gradient-based stochastic optimisation methods, e.g., (Kingma and Ba, 2015, Adam), we observe that the optimisation process is initially dominated by  $\bar{f}_{\phi}^{l,+}$ , likely because it contains one additional component  $\bar{f}_{\phi}^{L,+}$ . As training progresses, the gradient  $\nabla_{\phi} \bar{f}_{\phi}^{l,+}$  diminishes, and  $\nabla_{\phi} \bar{f}_{\phi}^{l,-}$  begins to dominate, causing an increase in  $\bar{f}_{\phi}^{l,+}$  and a decrease in  $\bar{f}_{\phi}^{l,-}$ ; see Figure 7. This dynamic results in a ‘‘tug-of-war’’ between the two components, ultimately leading to unstable gradients and the loss to diverge. Broadly speaking, the core idea behind MLMC is to approximate the objective using  $h_0(\phi) = \bar{f}_{\phi}^{0,+}$ , with subsequent terms serving as corrections. This extends to the optimisation as well: the gradient is primarily determined by  $\nabla_{\phi} h_0(\phi) = \nabla_{\phi} \bar{f}_{\phi}^{0,+}$ , while the corrections are captured by  $\nabla_{\phi} h_l(\phi) = \nabla_{\phi} \bar{f}_{\phi}^{l,+} + \nabla_{\phi} \bar{f}_{\phi}^{l-1,-}$ . Under seed matching, we expect  $f_{\phi}^l \approx f_{\phi}^{l-1}$ , which implies  $\bar{f}_{\phi}^{l,+} \approx -\bar{f}_{\phi}^{l-1,-}$  and  $\nabla_{\phi} \bar{f}_{\phi}^{l,+} \approx -\nabla_{\phi} \bar{f}_{\phi}^{l-1,-}$ , allowing  $\nabla_{\phi} h_l(\phi)$  to remain small and act as a correction to  $\nabla_{\phi} h_0(\phi)$  throughout the optimisation. However, in practice, this behaviour does not hold when standard gradient descent is applied naively due to the unbalance in the evolution of the gradient over the training epochs.

To address this, we apply two modifications. First, we rescale the gradients in the correction terms to ensure  $\|\bar{f}_{\phi}^{l,+}\| \approx \|\bar{f}_{\phi}^{l-1,-}\|$  for all  $l = 1, \dots, L$ , so that  $\nabla_{\phi} h_l(\phi)$  remains small and consistent with its intended role. See Figure 6 for the illustration in the case of two levels. Note that for two levels, we have  $\ell_{\text{MLMC}}(\phi) = h_0(\phi) + \bar{f}_{\phi}^{1,+} + \bar{f}_{\phi}^{1,-}$ . Second, we incorporate gradient surgery (Liu et al., 2020) to further facilitate optimisation with conflicting objectives. Specifically, when the dot product  $\nabla_{\phi} h_0(\phi) \cdot \nabla_{\phi} h_c(\phi) < 0$ , where  $\nabla_{\phi} h_c(\phi) := \sum_{l=1}^L \nabla_{\phi} h_l(\phi)$ , we project each gradient onto the normal plane of the other to remove the conflicting components. We empirically observe that combining these two steps improves the stability of gradient and optimisation throughout the training. Full algorithm is provided in Algorithm 1.

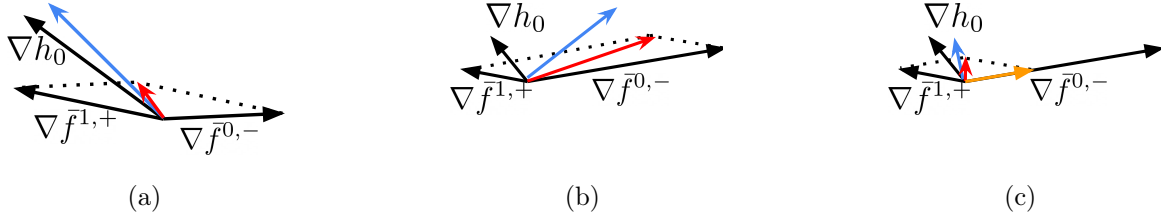


Figure 6: Illustration of the gradient scaling with two levels. The coloured arrows indicate **gradient of the correction term** (red), **total gradient** (blue), and **scaled gradient** (orange) respectively. (a) Ideal case:  $\|\nabla_{\phi} h_c(\phi)\|$  remains small and works as a correction to  $\nabla_{\phi} h_0(\phi)$ . (b) In the later stage of training,  $\nabla_{\phi} h_0(\phi)$  and  $\nabla_{\phi} \bar{f}_{\phi}^{1,+}$  diminishes and  $\nabla_{\phi} \bar{f}_{\phi}^{0,-}$  starts to dominate the optimisation. (c) Gradient scale adjustment: We scale  $\nabla_{\phi} \bar{f}_{\phi}^{0,-}$  such that  $\|\bar{f}_{\phi}^{1,+}\| \approx \|\bar{f}_{\phi}^{0,-}\|$  and  $\|\nabla_{\phi} h_c(\phi)\|$  remains small throughout the training as intended.

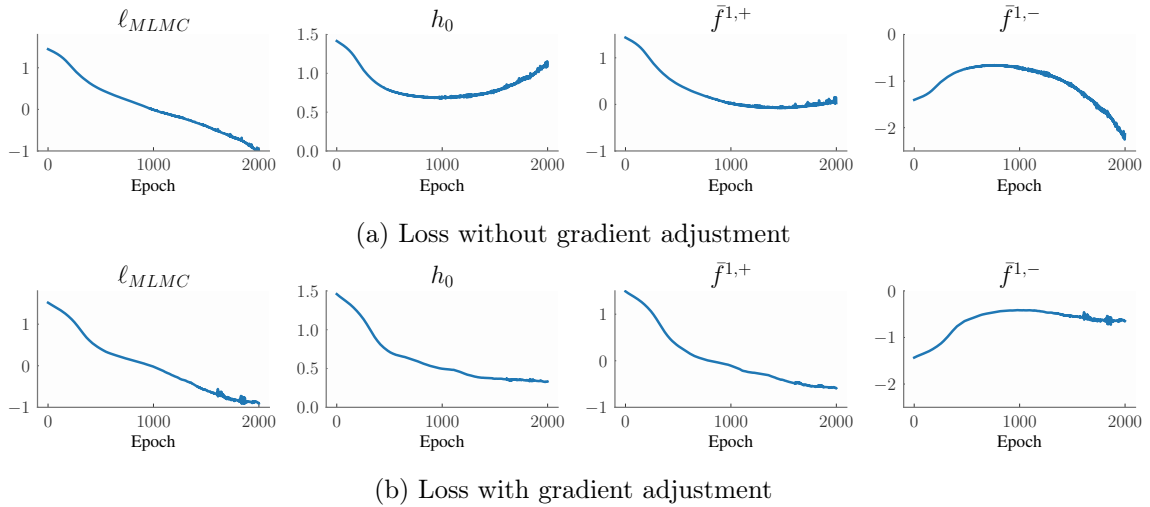


Figure 7: Comparison of training losses with and without gradient adjustment. (a) Without gradient adjustment, the contribution of  $\bar{f}_{\phi}^{1,-}$  begins to dominate the loss around epoch 1000. The resulting conflict between gradient components leads to unstable optimisation, as evidenced by strong fluctuations in the loss and eventual divergence of  $\bar{f}_{\phi}^{1,-}$ . (b) With gradient adjustment, all components contribute more stably, and the overall loss decreases steadily eventually, indicating convergence. Loss functions are shown for the g-and-k experiment with NLE.

---

**Algorithm 1** MLMC gradient adjustment
 

---

```

1: Input  $\nabla h_0(\phi), \{\nabla \bar{f}_\phi^{l,+}, \nabla \bar{f}_\phi^{l-1,-}\}_{l=1}^L$ 
2: for  $l = 1$  to  $L$  do
3:    $\nabla \bar{f}_\phi^{l-1,-} \leftarrow \frac{\|\nabla \bar{f}_\phi^{l,+}\|_2}{\|\nabla \bar{f}_\phi^{l-1,-}\|_2 + \epsilon} \nabla \bar{f}_\phi^{l-1,-}$ 
4: end for
5:  $\nabla h_c(\phi) \leftarrow \sum_{l=1}^L (\nabla \bar{f}_\phi^{l,+} + \nabla \bar{f}_\phi^{l-1,-})$ 
6: if  $\nabla h_0(\phi) \cdot \nabla h_c(\phi) < 0$  then
7:    $\tilde{\nabla} h_0(\phi) \leftarrow \nabla h_0(\phi) - \frac{\nabla h_0(\phi) \cdot \nabla h_c(\phi)}{\|\nabla h_c(\phi)\|_2^2} \nabla h_c(\phi)$ 
8:    $\tilde{\nabla} h_c(\phi) \leftarrow \nabla h_c(\phi) - \frac{\nabla h_0(\phi) \cdot \nabla h_c(\phi)}{\|\nabla h_0(\phi)\|_2^2} \nabla h_0(\phi)$ 
9: else  $\tilde{\nabla} h_0(\phi) \leftarrow \nabla h_0(\phi), \tilde{\nabla} h_1(\phi) \leftarrow \nabla h_1(\phi)$ 
10: end if
11: Output  $\tilde{\nabla} \ell_{\text{MLMC}}(\phi) \leftarrow \tilde{\nabla} h_0(\phi) + \tilde{\nabla} h_c(\phi)$ 

```

---

## B Proof of theoretical results

### B.1 Proof of Theorem 1

*Proof.* Note that here, and throughout the rest of this proof, we will simplify the notation. We will drop the subscript for variances and expectations, and these should all be understood as being  $u_{1:m} \sim \mathbb{U}^m$  and  $\theta \sim \pi$ . We will also use the variable  $z$  to denote a vector containing  $u_{1:m}$  and  $\theta$ , so that  $z \in \mathbb{R}^{m d_u + d_\theta}$  and  $z_i$  represents a vector containing  $u_{1:m,i}$  and  $\theta_i$ . Finally, we will write  $L^4$  and  $W^{1,4}$  to denote the weighted norms  $L^4(\pi \times \mathbb{U}^m)$  and  $W^{1,4}(\pi \times \mathbb{U}^m)$ .

The proof will be structured as follows. We will express the variance of each term using the variance of individual samples. We will then use a Poincaré-type inequality to bound the variance of the objective in terms of the expected squared norm of its gradient, then we will upper bound the norm using only terms which depend on constants and terms expressing how well  $G^{l-1}$  approximates  $G^l$ . Note that we will first prove the result for NLE, and will comment on the NPE case at the bottom of the proof.

Since each term in the MLMC expansion are MC estimators (and therefore based on independent samples), we can express the variances of each term as follows:

$$\begin{aligned}
 \text{Var}[h_0(\phi)] &= \text{Var}\left[\frac{1}{n_0} \sum_{i=1}^{n_0} f_\phi^0(z_i)\right] \\
 &= \frac{1}{n_0^2} \sum_{i=1}^{n_0} \text{Var}[f_\phi^0(z_i)] = \frac{1}{n_0} \text{Var}[f_\phi^0(z)],
 \end{aligned} \tag{5}$$

where we use the fact that the variance of a sum of independent random variables is the sum of variances. Similarly for the other levels,

$$\text{Var}[h_l(\phi)] = \frac{1}{n_l} \text{Var}\left[f_\phi^l(z) - f_\phi^{l-1}(z)\right] \quad \text{for } l \in \{1, \dots, L\}. \tag{6}$$

For the first step, we use a version of a Poincaré-type inequality for log-concave measures due to (Bobkov, 1999) (note that a simpler statement and additional discussion is provided

in Proposition 10.1 (b) of [Saumard and Wellner \(2014\)](#) for the case of strongly log-concave measures). This result shows that for any log-concave measure  $\mu$ , there exists  $K_{\text{Poin}} > 0$  such that for any sufficiently regular integrand  $f : \mathcal{Z} \rightarrow \mathbb{R}$  where  $\mathcal{Z} \subseteq \mathbb{R}^{dz}$ ,  $\text{Var}[f(z)] \leq K_{\text{Poin}} \mathbb{E}_{z \sim \mu} [\|\nabla f(z)\|_2^2]$ . Applying this Poincaré inequality to each term of the learning objective (i.e. to the terms in (5) and (6)), we get

$$\text{Var}[f_\phi^0(z)] \leq K_{\text{Poin}} \mathbb{E} \left[ \|\nabla_z f_\phi^0(z)\|_2^2 \right] \quad (7)$$

$$\text{Var}[f_\phi^l(z) - f_\phi^{l-1}(z)] \leq K_{\text{Poin}} \mathbb{E} \left[ \left\| \nabla_z f_\phi^l(z) - \nabla_z f_\phi^{l-1}(z) \right\|_2^2 \right] \quad (8)$$

for  $l \in \{1, \dots, L\}$ . Here, we emphasise again that the expectation is over  $z$ , which encompasses both  $\theta$  and  $u_{1:m}$ . This result requires the joint distribution of the prior  $\pi$  and  $m$  times the base measure  $\mathbb{U}$  to be log-concave, which holds since the product of log-concave densities is also log-concave (since the sum of convex functions is convex) and we have assumed that the prior and base measures are independent and separately log-concave through Assumption (A1).

To simplify notation, we now introduce the vector-valued function  $g^l(z) = g^l(\theta, u_{1:m}) = (G_\theta^l(u_1)^\top, \dots, G_\theta^l(u_m)^\top, \theta)^\top$  so that  $q_\phi^{\text{NLE}}(G_\theta^l(u) | \theta) = q_\phi^{\text{NLE}}(g^l(\theta, u)) = q_\phi^{\text{NLE}}(g^l(z))$ . We will now derive our first bound, which looks at the first term in the MLMC expansion. To do so, we simplify (7) as follows

$$\begin{aligned} \mathbb{E} \left[ \|\nabla_z f_\phi^0(z)\|_2^2 \right] &= \mathbb{E} \left[ \|\nabla_z \log q_\phi^{\text{NLE}}(g^0(z))\|_2^2 \right] \\ &= \mathbb{E} \left[ \|\nabla_z g^0(z) \nabla \log q_\phi^{\text{NLE}}(g^0(z))\|_2^2 \right] \end{aligned} \quad (9)$$

$$\leq \mathbb{E} \left[ \|\nabla_z g^0(z)\|_2^2 \|\nabla \log q_\phi^{\text{NLE}}(g^0(z))\|_2^2 \right] \quad (10)$$

$$\leq \mathbb{E} \left[ \|\nabla_z g^0(z)\|_2^4 \right]^{\frac{1}{2}} \mathbb{E} \left[ \|\nabla \log q_\phi^{\text{NLE}}(g^0(z))\|_2^4 \right]^{\frac{1}{2}} \quad (11)$$

Here, we have that (9) follows due to the chain rule, (10) follows due to the Cauchy-Schwarz inequality of the 2-norm, (11) follows due to the Cauchy-Schwarz inequality of expectations.

We now bound each term in (11) separately. For the first term, we get

$$\mathbb{E} \left[ \|\nabla_z g^0(z)\|_2^4 \right] = 2\mathbb{E} \left[ \|\nabla_z G^0(z)\|_2^4 \right] + 2\mathbb{E} \left[ \|\nabla_z \theta\|_2^4 \right] \quad (12)$$

$$\leq 2\mathbb{E} \left[ \|\nabla_z G^0(z)\|_F^4 \right] + 2\mathbb{E} \left[ \|\nabla_z \theta\|_F^4 \right] \quad (13)$$

$$= 2\mathbb{E} \left[ \left( \sum_{|\alpha|=1} \left( \sum_{j=1}^d (D^\alpha (G^0(z)))_j \right)^2 \right) \right]^2 + 2d_\Theta^2 \quad (14)$$

$$\leq 2(d_\Theta + md_\mathcal{U}) \sum_{|\alpha|=1} \mathbb{E} \left[ \left( \sum_{j=1}^d (D^\alpha (G^0(z)))_j \right)^2 \right]^2 + 2d_\Theta^2 \quad (15)$$

$$\leq 2(d_\Theta + md_\mathcal{U}) \sum_{|\alpha|=1} \mathbb{E} \left[ \|D^\alpha G^0(z)\|_2^4 \right] + 2d_\Theta^2 \quad (16)$$

$$\leq 2(d_\Theta + md_\mathcal{U}) \sum_{|\alpha|=1} \|D^\alpha G^0\|_{L^4}^4 + 2d_\Theta^2 \quad (17)$$

$$\leq 2(d_\Theta + md_\mathcal{U}) \|G^0\|_{W^{1,4}}^4 + 2d_\Theta^2, \quad (18)$$

$$\leq K_{\text{grad}} \left( \|G^0\|_{W^{1,4}}^4 + 1 \right) \quad (19)$$

where (12) follows from the fact that  $(a+b)^2 \leq 2a^2 + 2b^2$ , (13) follows from the fact that the Frobenius norm  $\|\cdot\|_F$  is an upper-bound on the matrix 2-norm, (14) follows from the definition of the Frobenius norm and from the fact that  $\mathbb{E}[\|\nabla_z \theta\|_F^4] = d_\Theta^2$ , (15) follows from the fact that  $(\sum_{i=1}^n a_i)^2 \leq n \sum_{i=1}^n a_i^2$ , and (16), (17) and (19) follow from the definitions of the 2-norm, the  $L^4$ -norm and the  $W^{1,4}$ -norm respectively.

We now move on to bounding the second term in (11). Since we assumed in Assumption (A3) that  $\nabla \log q_\phi^{\text{NLE}}$  satisfies a linear growth condition, we must have that

$$\mathbb{E} \left[ \|\nabla \log q_\phi^{\text{NLE}}(g^0(z))\|_2^4 \right] = \mathbb{E} \left[ \|\nabla \log q_\phi^{\text{NLE}}(G_\theta^0(u) | \theta)\|_2^4 \right] \quad (20)$$

$$\leq K_{\text{grow}}^4(\phi) \mathbb{E} \left[ (\|G^0(z)\|_2 + \|\theta\|_2 + 1)^4 \right] \quad (21)$$

$$\leq 27K_{\text{grow}}^4(\phi) \left( \mathbb{E} \left[ \|G^0(z)\|_2^4 \right] + \mathbb{E} \left[ \|\theta\|_2^4 \right] + 1 \right) \quad (22)$$

$$\leq 27K_{\text{grow}}^4(\phi) \left( \|G^0\|_{W^{1,4}}^4 + \mathbb{E} \left[ \|\theta\|_2^4 \right] + 1 \right)$$

$$\leq K_{\text{score}}(\phi) \left( \|G^0\|_{W^{1,4}}^4 + 1 \right) \quad (23)$$

Here, (21) uses the growth condition, (22) holds due since  $(a+b+c)^4 \leq 27(a^4 + b^4 + c^4)$ , and (23) uses the definition of Sobolev norm and the fact that  $\mathbb{E}[\|\theta\|_2^4]$  is upper bounded by a constant since the expectation is against  $\pi$ , which a log-concave distribution and hence all its moments are finite (see Section 5.1. of [Saumard and Wellner \(2014\)](#)). Combining (5), (7), (11), (19), and (23) therefore gives:

$$\begin{aligned} \text{Var} [h_0(\phi)] &\leq \frac{1}{n_0} K_{\text{Poin}} K_{\text{grad}}^{\frac{1}{2}} \left( \|G^0\|_{W^{1,4}}^4 + 1 \right)^{\frac{1}{2}} K_{\text{score}}(\phi)^{\frac{1}{2}} \left( \|G^0\|_{W^{1,4}}^4 + 1 \right)^{\frac{1}{2}} \\ &\leq \frac{K_0(\phi)}{n_0} \left( \|G^0\|_{W^{1,4}}^4 + 1 \right) \end{aligned} \quad (24)$$

where  $K_0(\phi)$  is used to combine all of the constants. This now concludes the first part of our results, which bounds the variance of the first term in the MLMC telescoping sum.

We can now derive a similar bound for the other terms (i.e. to simplify (8)). We do this by first only considering the norm inside of the expectation:

$$\begin{aligned} & \left\| \nabla_z f_\phi^l(z) - \nabla_z f_\phi^{l-1}(z) \right\|_2 \\ &= \left\| \nabla_z \log q_\phi^{\text{NLE}}(g^l(z)) - \nabla_z \log q_\phi^{\text{NLE}}(g^{l-1}(z)) \right\|_2 \\ &= \left\| \nabla_z g^l(z) \nabla \log q_\phi^{\text{NLE}}(g^l(z)) - \nabla_z g^{l-1}(z) \nabla \log q_\phi^{\text{NLE}}(g^{l-1}(z)) \right\|_2 \end{aligned} \quad (25)$$

$$\begin{aligned} & \leq \left\| \nabla_z g^l(z) \left( \nabla \log q_\phi^{\text{NLE}}(g^l(z)) - \nabla \log q_\phi^{\text{NLE}}(g^{l-1}(z)) \right) \right\|_2 \\ & \quad + \left\| \left( \nabla_z g^l(z) - \nabla_z g^{l-1}(z) \right) \nabla \log q_\phi^{\text{NLE}}(g^{l-1}(z)) \right\|_2 \end{aligned} \quad (26)$$

$$\begin{aligned} & \leq \left\| \nabla_z g^l(z) \right\|_2 \left\| \nabla \log q_\phi^{\text{NLE}}(g^l(z)) - \nabla \log q_\phi^{\text{NLE}}(g^{l-1}(z)) \right\|_2 \\ & \quad + \left\| \nabla_z g^l(z) - \nabla_z g^{l-1}(z) \right\|_2 \left\| \nabla \log q_\phi^{\text{NLE}}(g^{l-1}(z)) \right\|_2 \end{aligned} \quad (27)$$

Here, (25) follows from the chain rule, (26) follows by adding and subtracting the term  $\nabla_z g^l(z) \nabla \log q_\phi^{\text{NLE}}(g^{l-1}(z))$  and using the triangle inequality, and (27) follows from the Cauchy-Schwarz inequality of the 2-norm. Squaring both sides of this inequality and taking expectations, we then obtain:

$$\begin{aligned} & \mathbb{E} \left[ \left\| \nabla_z f_\phi^l(z) - \nabla_z f_\phi^{l-1}(z) \right\|_2^2 \right] \\ & \leq \mathbb{E} \left[ \left( \left\| \nabla_z g^l(z) \right\|_2 \left\| \nabla \log q_\phi^{\text{NLE}}(g^l(z)) - \nabla \log q_\phi^{\text{NLE}}(g^{l-1}(z)) \right\|_2 \right. \right. \\ & \quad \left. \left. + \left\| \nabla_z g^l(z) - \nabla_z g^{l-1}(z) \right\|_2 \left\| \nabla \log q_\phi^{\text{NLE}}(g^{l-1}(z)) \right\|_2 \right)^2 \right] \\ & \leq \mathbb{E} \left[ 2 \left\| \nabla_z g^l(z) \right\|_2^2 \left\| \nabla \log q_\phi^{\text{NLE}}(g^l(z)) - \nabla \log q_\phi^{\text{NLE}}(g^{l-1}(z)) \right\|_2^2 \right. \\ & \quad \left. + 2 \left\| \nabla_z g^l(z) - \nabla_z g^{l-1}(z) \right\|_2^2 \left\| \nabla \log q_\phi^{\text{NLE}}(g^{l-1}(z)) \right\|_2^2 \right]. \end{aligned} \quad (28)$$

$$\begin{aligned} & \leq 2\mathbb{E} \left[ \left\| \nabla_z g^l(z) \right\|_2^4 \right]^{\frac{1}{2}} \mathbb{E} \left[ \left\| \nabla \log q_\phi^{\text{NLE}}(g^l(z)) - \nabla \log q_\phi^{\text{NLE}}(g^{l-1}(z)) \right\|_2^4 \right]^{\frac{1}{2}} \\ & \quad + 2\mathbb{E} \left[ \left\| \nabla_z g^l(z) - \nabla_z g^{l-1}(z) \right\|_2^4 \right]^{\frac{1}{2}} \mathbb{E} \left[ \left\| \nabla \log q_\phi^{\text{NLE}}(g^{l-1}(z)) \right\|_2^4 \right]^{\frac{1}{2}}. \end{aligned} \quad (29)$$

where (28) follows from that fact that for  $a, b \in \mathbb{R}$ , we have  $(a + b)^2 \leq 2a^2 + 2b^2$ , and (29) follows from the Cauchy-Schwarz inequality for expectations. To conclude this proof, we notice that the derivation from (13) to (19) can be modified by replacing  $G^0$  by  $G^l$  to get:

$$\mathbb{E} \left[ \left\| \nabla_z g^l(z) \right\|_2^4 \right] \leq K_{\text{grad}} \left( \left\| G^l \right\|_{W^{1,4}}^4 + 1 \right) \leq K_{\text{grad}} (S_l^4 + 1). \quad (30)$$

where the last inequality holds thanks to Assumption (A2). Similarly, replacing  $G^0$  by  $G^l - G^{l-1}$  gives

$$\mathbb{E} \left[ \left\| \nabla_z g^l(z) - \nabla_z g^{l-1}(z) \right\|_2^4 \right] \leq K_{\text{grad}} \left( \left\| G^l - G^{l-1} \right\|_{W^{1,4}}^4 + 1 \right). \quad (31)$$

Additionally, we could replace  $G^0$  by  $G^{l-1}$  in the the bound from (21) to (23) in order to get:

$$\mathbb{E} \left[ \left\| \nabla \log q_\phi^{\text{NLE}} \left( g^{l-1}(z) \right) \right\|_2^4 \right] \leq K_{\text{score}}(\phi) \left( \left\| G^{l-1} \right\|_{W^{1,4}}^4 + 1 \right) \quad (32)$$

$$\leq K_{\text{score}}(\phi) (S_{l-1}^4 + 1) \quad (33)$$

where once again we used Assumption (A2).

Finally, we split the following expression to make use of our local Lipschitz property:

$$\mathbb{E} \left[ \left\| \nabla \log q_\phi^{\text{NLE}} \left( g^l(z) \right) - \nabla \log q_\phi^{\text{NLE}} \left( g^{l-1}(z) \right) \right\|_2^4 \right] \quad (34)$$

$$\begin{aligned} &= \mathbb{E} \left[ \left\| \nabla \log q_\phi^{\text{NLE}} \left( g^l(z) \right) - \nabla \log q_\phi^{\text{NLE}} \left( g^{l-1}(z) \right) \right\|_2^4 \mid \left\| G^l(z) - G^{l-1}(z) \right\|_2 \geq \delta \right] \\ &\quad \times \mathbb{P} \left[ \left\| G^l(z) - G^{l-1}(z) \right\|_2 \geq \delta \right] \\ &+ \mathbb{E} \left[ \left\| \nabla \log q_\phi^{\text{NLE}} \left( g^l(z) \right) - \nabla \log q_\phi^{\text{NLE}} \left( g^{l-1}(z) \right) \right\|_2^4 \mid \left\| G^l(z) - G^{l-1}(z) \right\|_2 < \delta \right] \\ &\quad \times \mathbb{P} \left[ \left\| G^l(z) - G^{l-1}(z) \right\|_2 < \delta \right] \end{aligned} \quad (35)$$

$$\begin{aligned} &\leq \frac{16}{\delta} \left( \mathbb{E} \left[ \left\| \nabla \log q_\phi^{\text{NLE}} \left( g^l(z) \right) \right\|_2^4 \right] + \mathbb{E} \left[ \left\| \nabla \log q_\phi^{\text{NLE}} \left( g^{l-1}(z) \right) \right\|_2^4 \right] \right) \mathbb{E} \left[ \left\| G^l(z) - G^{l-1}(z) \right\|_2 \right] \\ &\quad + K_{\text{Lip}}(\phi)^4 \mathbb{E} \left[ \left\| g^l(z) - g^{l-1}(z) \right\|_2^4 \right] \times 1 \end{aligned} \quad (36)$$

$$\leq K_{\text{score-diff}}(\phi, \delta) \left\| G^l - G^{l-1} \right\|_{W^{1,4}}^4 \quad (37)$$

where (35) follows due to the law of total expectation. For (36), the bound on the first term follows due to the triangle inequality and Markov's inequality, and the bound on the second term follows due to the local-Lipschitz condition (i.e. Assumption (A3)) and the fact that a probability is always upper bounded by 1. Finally, (37) follows using (33) and the definition of Sobolev norm, and by grouping all constants. Combining all of the above (i.e. (6), (8), (27), (30), (31), (33), and (37)), we end up with

$$\begin{aligned} \text{Var} [h_l(\phi)] &\leq \frac{2}{n_l} K_{\text{Poin}} \left( K_{\text{grad}}^{\frac{1}{2}} (S_l^4 + 1)^{\frac{1}{2}} K_{\text{score-diff}}^{\frac{1}{2}}(\phi, \delta) \left\| G^l - G^{l-1} \right\|_{W^{1,4}}^2 \right. \\ &\quad \left. + K_{\text{grad}}^{\frac{1}{2}} \left( \left\| G^l - G^{l-1} \right\|_{W^{1,4}}^4 + 1 \right)^{\frac{1}{2}} K_{\text{score}}(\phi)^{\frac{1}{2}} (S_{l-1}^4 + 1)^{\frac{1}{2}} \right) \\ &\leq \frac{K_l(\phi)}{n_l} \left( \left\| G^l - G^{l-1} \right\|_{W^{1,4}}^2 + 1 \right), \end{aligned}$$

where  $K_l(\phi)$  combines all constants. This proves our second result and therefore concludes our proof.

Note that the proof follows analogously for NPE with the alternative locally-Lipschitz and growth condition assumptions.  $\square$

## B.2 Proof of Theorem 2

*Proof.* We first recall both the cost and the variance of our estimator, modifying our notation slightly to emphasise the number of samples  $n_0, \dots, n_L$ . The total cost of this method is

given by

$$\text{Cost}(\ell_{\text{MLMC}}(\phi); n_0, \dots, n_L) = n_0 C_0 + \sum_{l=1}^L n_l (C_l + C_{l-1}),$$

where  $C_l$  is the cost of evaluating  $f^l$  at level  $l$ . In addition, we also have the following upper bound on the variance using Theorem 1:

$$\text{Var}[\ell_{\text{MLMC}}(\phi); n_0, \dots, n_L] \leq \frac{K_0(\phi)}{n_0} \left( \|G^0\|_{W^{1,4}}^4 + 1 \right) + \sum_{l=1}^L \frac{K_l(\phi)}{n_l} \left( \|G^l - G^{l-1}\|_{W^{1,4}}^2 + 1 \right),$$

where once again we write  $\|\cdot\|_{W^{1,4}}$  to denote the weighted norm  $\|\cdot\|_{W^{1,4}(\pi \times \mathbb{U})}$ . Overall, we would like to solve the following optimisation problem:

$$\begin{aligned} (n_0^*, \dots, n_L^*)^\top &:= \arg \min_{(n_0, \dots, n_L)^\top} \text{Var}[\ell_{\text{MLMC}}(\phi); n_0, \dots, n_L] \\ &\text{such that } \text{Cost}(\ell_{\text{MLMC}}(\phi); n_0, \dots, n_L) \leq C_{\text{budget}}, \end{aligned}$$

where  $C_{\text{budget}}$  is the computational budget. We relax the problem slightly by minimising the upper bound on the variance instead, thus the problem can be expressed in the following Lagrangian form:

$$\begin{aligned} \mathcal{L}(n_0, \dots, n_L, \nu) &:= \frac{K_0(\phi)}{n_0} \left( \|G^0\|_{W^{1,4}}^4 + 1 \right) + \sum_{l=1}^L \frac{K_l(\phi)}{n_l} \left( \|G^l - G^{l-1}\|_{W^{1,4}}^2 + 1 \right) \\ &\quad + \nu \left( \text{Cost}(\ell_{\text{MLMC}}(\phi); n_0, \dots, n_L) - C_{\text{budget}} \right) \\ &= \frac{K_0(\phi)}{n_0} \left( \|G^0\|_{W^{1,4}}^4 + 1 \right) + \sum_{l=1}^L \frac{K_l(\phi)}{n_l} \left( \|G^l - G^{l-1}\|_{W^{1,4}}^2 + 1 \right) \\ &\quad + \nu \left( n_0 C_0 + \sum_{l=1}^L n_l (C_l + C_{l-1}) - C_{\text{budget}} \right). \end{aligned}$$

This can be solved by setting all partial derivatives with respect to  $(n_0, \dots, n_L)$  and  $\nu$  equal to zero and solving the associated system of equations. Firstly, we get:

$$\frac{\partial \mathcal{L}(n_0, \dots, n_L, \nu)}{\partial n_0} = -K_0(\phi) \left( \|G^0\|_{W^{1,4}}^4 + 1 \right) n_0^{-2} + \nu C_0 = 0 \quad (38)$$

$$\Leftrightarrow n_0^* = \sqrt{\frac{K_0(\phi)}{\nu C_0} \left( \|G^0\|_{W^{1,4}}^4 + 1 \right)}, \quad (39)$$

and for  $l \in \{1, \dots, L\}$ , we have:

$$\begin{aligned} \frac{\partial \mathcal{L}(n_0, \dots, n_L, \nu)}{\partial n_l} &= -K_l(\phi) \left( \|G^l - G^{l-1}\|_{W^{1,4}}^2 + 1 \right) n_l^{-2} + \nu (C_l + C_{l-1}) = 0 \\ \Leftrightarrow n_l^* &= \sqrt{\frac{K_l(\phi)}{\nu (C_l + C_{l-1})} \left( \|G^l - G^{l-1}\|_{W^{1,4}}^2 + 1 \right)}. \end{aligned} \quad (40)$$

Finally, taking the partial derivative with respect to  $\nu$  confirms that our constraint is active (i.e. we are on the boundary of the feasible region):

$$\begin{aligned} \frac{\partial L(n_0, \dots, n_L, \nu)}{\partial \nu} &= n_0 C_0 + \sum_{l=1}^L n_l (C_l + C_{l-1}) - C_{\text{budget}} = 0 \\ \Leftrightarrow C_{\text{budget}} &= n_0 C_0 + \sum_{l=1}^L n_l (C_l + C_{l-1}). \end{aligned} \quad (41)$$

Plugging the results of (39) and (40) into (41), we get:

$$\begin{aligned} C_{\text{budget}} &= n_0 C_0 + \sum_{l=1}^L n_l (C_l + C_{l-1}) \\ &= \sqrt{\frac{K_0(\phi)}{\nu C_0} (\|G^0\|_{W^{1,4}}^4 + 1)} \times C_0 + \sum_{l=1}^L \sqrt{\frac{K_l(\phi)}{\nu (C_l + C_{l+1})} (\|G^l - G^{l-1}\|_{W^{1,4}}^2 + 1)} \times (C_l + C_{l-1}) \\ &= \nu^{-\frac{1}{2}} \left( \sqrt{K_0(\phi) C_0 (\|G^0\|_{W^{1,4}}^4 + 1)} + \sum_{l=1}^L \sqrt{K_l(\phi) (C_l + C_{l+1}) (\|G^l - G^{l-1}\|_{W^{1,4}}^2 + 1)} \right), \end{aligned}$$

which gives

$$\nu = \frac{\left( \sqrt{K_0(\phi) C_0 (\|G^0\|_{W^{1,4}}^4 + 1)} + \sum_{l=1}^L \sqrt{K_l(\phi) (C_l + C_{l+1}) (\|G^l - G^{l-1}\|_{W^{1,4}}^2 + 1)} \right)^2}{C_{\text{budget}}^2}. \quad (42)$$

We can now use the expression for  $\nu$  that we obtained in (42) to obtain a simplified expression for  $n_0, \dots, n_L$  (using (39) and (40)):

$$n_0^* \propto \frac{C_{\text{budget}}}{\sqrt{C_0}} \sqrt{\|G^0\|_{W^{1,4}}^4 + 1}, \quad n_l^* \propto \frac{C_{\text{budget}}}{\sqrt{C_l + C_{l+1}}} \sqrt{\|G^l - G^{l-1}\|_{W^{1,4}}^2 + 1} \quad \text{for } l \in \{1, \dots, L\}.$$

This completes our proof.  $\square$

## C Experimental details & additional results

For all the experiments, we use a Mac M4 CPU with 16 GB memory for the training of neural networks. Running all the experiments roughly takes half a day. For optimisation, we use batch gradient descent with the Adam optimiser (Kingma and Ba, 2015) using Pytorch (Paszke et al., 2017). For the construction of the conditional density estimator, we use the SBI package (Tejero-Cantero et al., 2020). We also use the BayesFlow package (Radev et al., 2023b) for some of the figures. For each experiment, we fix the number of epochs unless stated otherwise. We use the same setting and stopping criterion for the NPE and the NLE baseline as in the default implementation of the SBI package. We set the learning rate to  $10^{-4}$  for all the experiments.

## C.1 The g-and-k distribution

**Simulator setup.** The g-and-k distribution can be written in simulator form as follows:

$$G_\theta(u) = \theta_1 + \theta_2 \left( 1 + 0.8 \left( \frac{1 - \exp(-\theta_3 z(u))}{1 + \exp(-\theta_3 z(u))} \right) \right) (1 + z(u)^2)^{\log(\theta_4)} z(u),$$

$$z(u) = \Phi^{-1}(u) = \sqrt{2} \operatorname{erf}^{-1}(2u - 1), \quad u \sim \operatorname{Unif}([0, 1]),$$

where  $\Phi^{-1}$  is the quantile function of the standard normal distribution and  $\operatorname{erf}^{-1}$  is the inverse of error function. We set the prior distribution to be a tensor product of marginal distributions on each parameter:  $\theta_1, \theta_2, \theta_3 \sim \operatorname{Unif}([0, 3]^3)$  and  $\theta_4 \sim \operatorname{Unif}([0, \exp(0.5)])$ . Note that we always resort to an approximation method for the evaluation of  $\operatorname{erf}^{-1}(\cdot)$ . For the high-fidelity simulator, we use an accurate approximation implemented in Scipy (Virtanen et al., 2020). For the low-fidelity simulator, we use a Taylor expansion of  $\operatorname{erf}^{-1}$  up to the third order:

$$z_{\text{low}}(u) := \sqrt{2} \operatorname{erf}_{\text{low}}^{-1}(2u - 1), \quad \operatorname{erf}_{\text{low}}^{-1}(v) := \frac{\pi}{2} \left( u + \frac{\pi}{12} u^3 \right).$$

An advantage of the g-and-k distribution is that its density can be approximated numerically almost exactly. Following Rayner and MacGillivray (2002), we first numerically obtain  $G_\theta^{-1}(x)$  by solving numerically for  $x_i - G_\theta(u_i) = 0$  using a root-solving algorithm (Press, 2007)<sup>1</sup>, then we obtain the density function by taking  $\hat{p}(x | \theta) := F'_\theta(x) = \partial F_\theta(x) / \partial x$ . For this second step, we typically use a finite difference approximation. Seed-matching is simply done by using same the  $u$  and  $\theta$ .

### Neural network details

**NLE:** We use the neural spline flow (NSF) (Durkan et al., 2019). We pick 10 bins, span of  $[-7, 7]$  and 1 coupling layer since we only have one dimensional input. The conditioner for the NSF is a multilayer perceptron neural network (MLP) with 3 hidden layers of 50 units, and 10% dropout, trained for 10,000 epochs.

**NPE:** We use NSF with 3 bins, span of  $[-3, 3]$  and 3 coupling layers. The conditioner for the NSF is a MLP with 2 hidden layers of 50 units, and 10% dropout, trained for 800 epochs. For each true parameter values, we produce  $m = 1000$  i.i.d samples and obtain quantile based 4-dimensional summary statistics following Prangle (2016).

### Evaluations details

**NLE:** We calculate the forward KL-divergence between the almost exact density and the approximated density over 2000 equidistant points in  $[-30, 30]$ .

---

<sup>1</sup>Note that since  $G_\theta(u)$  is a quantile function,  $F_\theta(x) := G_\theta^{-1}(x)$  is a cumulative distribution function.

**NPE:** We calculate NLPD over 500 simulations. Empirical coverage is estimated using average value of 500 simulated datasets, where we draw 2000 posterior samples from each simulations. We then calculate  $1 - \beta$ -highest posterior density credible interval, where  $\beta$  is 101 equidistant points between 0 and 1.

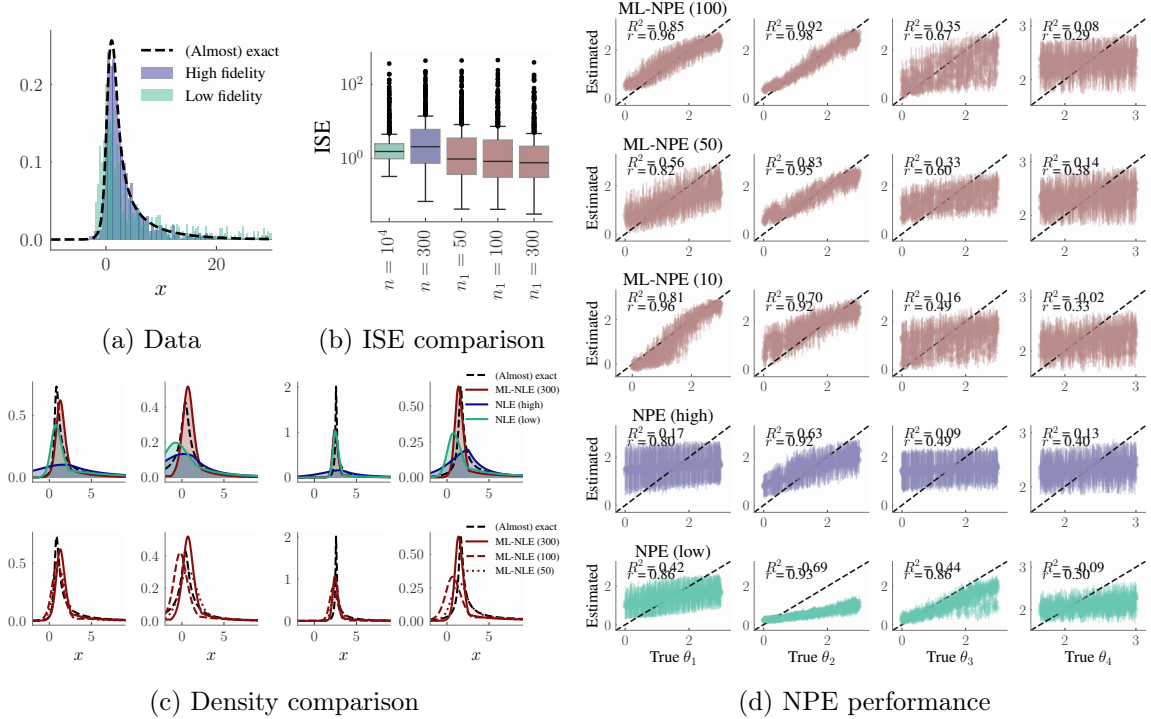


Figure 8: Additional results for the g-and-k experiment. (a) Histogram of 1000 seed-matched samples from low- and high-fidelity simulator. (b) ISE (integrated squared error) for NLE (↓): sum of the squared distance between (almost) exact density and approximated density over 2000 points in the interval  $[-30, 30]$ . The performance of ML-NLE improves as  $n_1$  increases. (c) Approximated density and (almost) exact density for NLE across four simulations. The first row of (c) shows that we get better approximation of the density when combining low and fidelity samples than using them separately. The second row of (c) shows the improvement of the performance of our ML-NLE as  $n_1$  increases. These results demonstrate the effectiveness of our method. (d) Recovery plot for NPE: It measures how well the ground truth value is captured by the median of approximated posterior. The x-axis shows the ground truth parameter value and the y-axis shows the median of the posterior distribution with the median absolute deviation, i.e.  $\pm \text{median}(|\theta - \text{median}(\theta)|)$ , shown around the points. Here  $r$  and  $R^2$  denotes the correlation coefficient (↑) and the coefficient of determination (↑) between the ground truth values and the estimated median, respectively. The dashed diagonal line indicates perfect recovery of the true parameter. Using MLMC leads to significant improvements in the parameter recovery, which become more pronounced as  $n_1$  increases.

## C.2 Training time comparison

We report training time per epoch for our multilevel versions of NLE and NPE and their standard counterparts for the g-and-k experiment; see Appendix C.2. For both methods, we

picked  $n = 2000$  for the standard NLE/NPE with MC loss and  $n_0 = 1000, n_1 = 500$  for our ML-NLE/ML-NPE with MLMC loss such that the total number of samples are the same. Each network is trained independently 10 times to assess uncertainty, with a training budget of 500 epochs for NLE and 100 epochs for NPE.

Table 1: Average training time per epoch (standard deviation in gray).

Method	Training Time per Epoch ( $s \times 10^{-3}$ )
ML-NLE	1.82 ( $\pm 0.05$ )
NLE	1.58 ( $\pm 0.06$ )
ML-NPE	8.04 ( $\pm 0.17$ )
NPE	6.56 ( $\pm 0.14$ )

### C.3 Ornstein–Uhlenbeck process

**Simulator setup.** Given  $T = 10$  (total time),  $\Delta t = 0.1$  (time step),  $x_0 = 2.0$  (initial value),  $\theta = [\gamma, \mu, \sigma]^\top$ ,  $N = \lfloor T/\Delta t \rfloor = 100$  (number of steps), the high- and the low-fidelity OUP simulators are defined as follows:

#### High fidelity:

For  $t = 0, \dots, N - 1$

$$x_{t+1} = x_t + \Delta x_t, \quad \Delta x_t = \gamma(\mu - x_t) + \sigma u_t \sqrt{\Delta t}, \quad u_t \sim \mathcal{N}(0, 1)$$

#### Low fidelity:

$$x_{1:N} = u_{1:N}(\sigma/\sqrt{2\gamma}) + \mu, \quad u_{1:N} \sim \mathcal{N}(0, 1)$$

We set the prior distribution  $\theta \sim \text{Unif}([0.1, 1.0] \times [0.1, 3.0] \times [0.1, 0.6])$ . The resulting  $x$  is a 100-dimensional time series. Seed-matching is simply done by using the same  $u$  and  $\theta$ .

**Neural network details.** We use NSF with 2 bins, span of  $[-2, 2]$  and 2 coupling layers. The conditioner for the NSF is a MLP with 1 hidden layer of 20 units, and 20% dropout. For ML-NPE, we trained the network for 500 epochs. For TL-NPE, we set a high maximum number of epochs and used on early stopping. The stopping criterion is based on the validation loss computed on 10% of the data, with a patience parameter controlling how many epochs to wait before stopping. For each true parameter values, we produce  $m = 1$  sample and use 5 representative data points as a summary statistics. The subsamples are taken at equal interval in log space such that we take 0, 3, 10, 31, 99th data points.

**Evaluations details.** We train each ML-NPE and TL-NPE 20 times hence the boxplot is over 20 data points. For each trained network, we compute the median NLPD across 500 simulated datasets. The use of the median, rather than the mean, is motivated by the presence of occasional extreme NLPD values in a few simulations. To estimate the

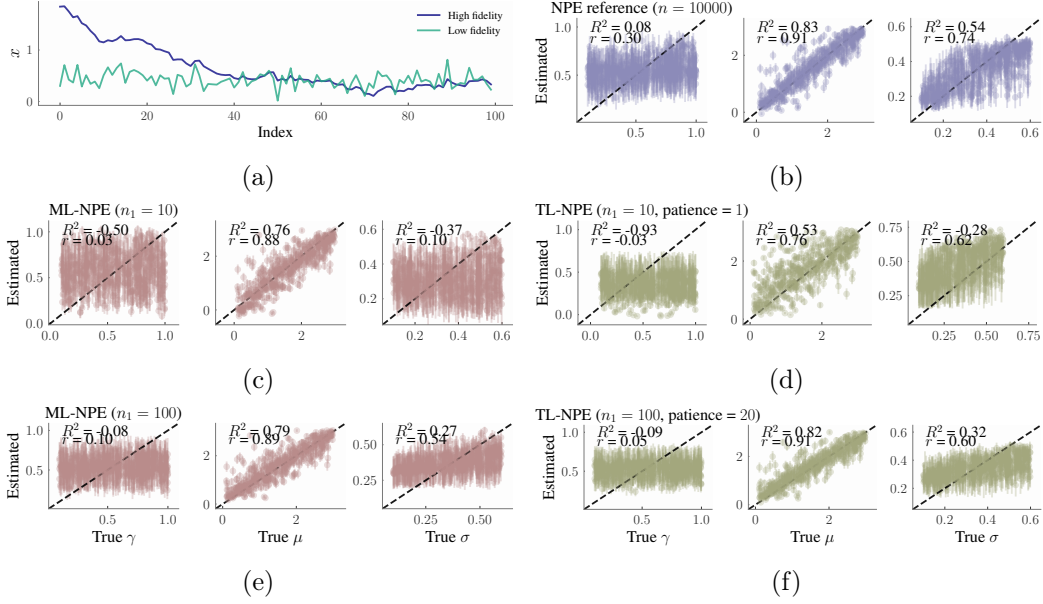


Figure 9: Additional results for the OUP experiment. (a) Example of one seed-matched sample from high and low fidelity simulators. (b) Recovery plot for the reference NPE posterior with  $n = 10^4$ . (c)-(f) Recovery plots for ML-NPE and TL-NPE for  $n_1 = 10$  and  $n_1 = 100$ . For TL-NLE, we picked the result corresponding to the best performing hyperparameter of their stopping criterion (i.e. patience = 1 for  $n_1 = 10$  and patience = 20 for  $n_1 = 100$ ) to visualise. For  $n_1 = 10$ , ML-NPE achieves better performance on  $\gamma$  and  $\mu$ . For  $n_1 = 100$ , it achieves superior performance on  $\gamma$  and competitive results on the remaining two. Recall that, unlike TL-NPE, ML-NPE does not have any hyperparameter to tune.

KLD, we draw 2000 samples from the reference density, and evaluate the densities at each sampled value of  $\theta$  for the both target and reference NPE, and compute the KLD for each simulation. The final KLD value for each network is obtained by averaging the results over 500 simulations.

#### C.4 Toggle switch model

**Simulator setup.** We follow the implementation by Key et al. (2025). Given parameters  $\theta = [\alpha_1, \alpha_2, \beta_1, \beta_2, \mu, \sigma, \gamma]^\top$ , we can sample from the simulator by  $x \sim \tilde{\mathcal{N}}(\mu + u_T, \mu\sigma/u_T^\gamma)$ , where  $\tilde{\mathcal{N}}$  denotes the truncated normal distribution on  $\mathbb{R}_+$ . Here,  $u_T$  is given by the discretised-time equation as follows:

For  $t = 0, \dots, T - 1$ :

$$u_{t+1} \sim \tilde{\mathcal{N}}(\mu_{u,t}, 0.5), \quad \mu_{u,t} = u_t + \frac{\alpha_1}{(1 + v_t^{\beta_1})} - (1 + 0.03u_t),$$

$$v_{t+1} \sim \tilde{\mathcal{N}}(\mu_{v,t}, 0.5), \quad \mu_{v,t} = v_t + \frac{\alpha_2}{(1 + u_t^{\beta_2})} - (1 + 0.03v_t)$$

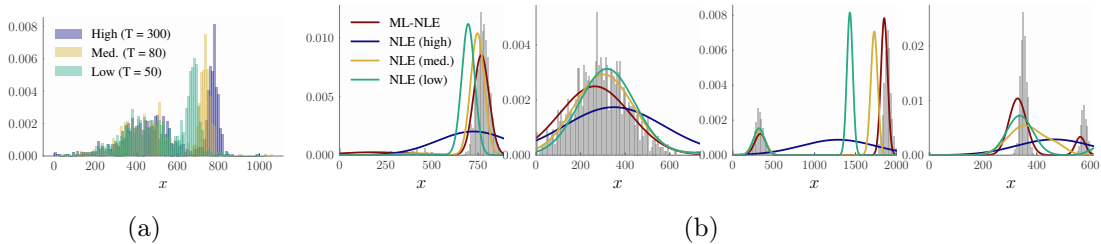


Figure 10: Additional results for the Toggle-switch experiment. (a) Histograms of 1000 seed-matched samples from the high-, the medium-, and the low-fidelity simulators. (b) Approximated density and samples from high-fidelity simulator across four simulations. ML-NLE demonstrates superior performance compared to the NLE baselines trained exclusively on high-, medium-, and low-fidelity data with same total simulation budget. In particular, the density estimated by ML-NLE aligns more closely with high-fidelity simulations, highlighting the improved accuracy of our method.

We set the initial state  $u_0 = u_1 = 10$  and prior distribution  $\theta \sim \text{Unif}([0.01, 50] \times [0.01, 50] \times [0.01, 5] \times [0.01, 5] \times [250, 450] \times [0.01, 0.5] \times [0.01, 0.4])$ . The cost of the simulator increases linearly with  $T$ , and  $T \rightarrow \infty$  leads to an exact simulation. Different choice of  $T$  leads to the simulator with different fidelity levels, having different cost and precision. The expression for the cost of simulating data for the MLMC and MC is given by

$$C_{\text{ML-NLE}} = c \left( n_0 T_0 + \sum_{l=1}^L n_l (T_l + T_{l-1}) \right) \quad \text{and} \quad C_{\text{NLE}} = c T n.$$

This yields a total data generation cost for ML-NLE with  $(n_0, n_1, n_2) = (10^4, 500, 300)$ ,  $(T_0, T_1, T_2) = (50, 80, 300)$  as  $C_{\text{MLMC}} = 60300$ , assuming a unit cost  $c = 1$ . We then allocate the same computational budget to NLE at different fidelities. This results in the following sample sizes:  $n_{\text{high}} = C_{\text{ML-NLE}}/T_2 = 2010$ ,  $n_{\text{med.}} = C_{\text{ML-NLE}}/T_1 = 7537$ , and  $n_{\text{low}} = C_{\text{ML-NLE}}/T_0 = 12060$ .

Note that  $\mathcal{U}$  varies with the fidelity level of the simulator, as it is given by  $\mathbb{R}^{2T+1}$ . This discrepancy can complicate seed matching across fidelities. To address this, we can define a unified domain for the noise  $\mathcal{U} = \bigcup_{l=0}^L \mathcal{U}^l$  shared across all fidelity levels, and assume that for lower fidelities (smaller  $l$ ), certain components of the input are simply disregarded. For seed matching, we share  $\theta$  and  $u_l \cap u_{l-1} = u_{l-1}$  where  $u_l \in \mathcal{U}^l \subseteq \mathcal{U}, \forall l$ .

**Neural network details.** We use Gaussian mixture density network (Bishop, 1994) with two mixture components. We use MLP with 2 hidden layers and 20 units to estimate the parameters: means, variances, and mixture weights, trained for 10,000 epochs.

**Evaluations details.** We sample  $m = 500$  from both high fidelity simulator and each approximated densities, and calculate MMD over 5000 simulations. The length scale is estimated by the median heuristic.

## C.5 Cosmological simulations

**Simulator setup.** We use the CAMELS simulation suite (Villaescusa-Navarro et al., 2021, 2023), a benchmark dataset for machine learning in astrophysics, to study multi-fidelity simulation-based inference in cosmology. The dataset includes both low-fidelity (gravity-only N-body) and high-fidelity (hydrodynamic) simulations of 25 Mpc/ $h$  cosmological volumes. The original inference task involves two cosmological parameters,  $\theta = (\Omega_m, \sigma_8)$ , where  $\Omega_m$  is the matter density and  $\sigma_8$  the amplitude of fluctuations, with mock power spectrum measurements  $P(k)$  used to infer the parameters. However, due to the limited availability of both high- and low-fidelity simulations, we focus on inferring only  $\sigma_8$  and treat  $\Omega_m$  as part of the nuisance parameter. We found that attempting to jointly infer both parameters led to poor performance (expected due to physical  $\sigma_8$ - $\Omega_m$  degeneracy) even when using 90% of the high-fidelity data.

In this setup, low-fidelity simulations are governed solely by  $\theta$  and the initial condition seed  $u$ , while high-fidelity simulations additionally incorporate complex astrophysical processes (e.g., feedback), modelled via four extra parameters. These high-fidelity simulations are significantly more computationally expensive—often more than  $100\times$  slower to generate than low-fidelity ones. Given these limitations, cosmological analyses often rely on conservative data cuts to exclude small-scale modes (e.g.,  $k \gtrsim 0.1, h/\text{Mpc}$ ), where simulation inaccuracies are most pronounced (e.g. Jeffrey et al., 2025; Gatti et al., 2025). Multi-fidelity approaches aim to mitigate such constraints by leveraging both inexpensive and high-fidelity simulations to improve the accuracy of cosmological inference.

Note that the idea of combining low- and high- fidelity simulations has previously been proposed in cosmology; see for example the work of Chartier et al. (2021); Chartier and Wandelt (2022) who use low-fidelity simulations to construct approximations of quantities of interest which can be used as control variates. This work differs from our proposed approach in that it is based on regression and approximations of quantities such as means and covariances of interest, rather than of the training objective of neural SBI.

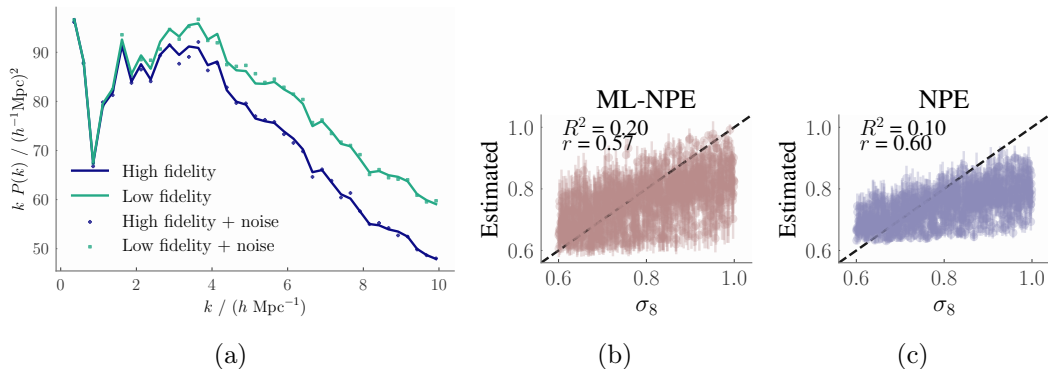


Figure 11: Additional results for the cosmological simulator experiment. The one with noise is used to train the neural networks. (a) 1 seed-matched sample from high and low fidelity simulators. (b)-(c) Recovery plot of ML-NPE and NPE. Adding low fidelity samples lead better recovery of the parameter.

**Neural network details.** We use NSF with 3 bins, span of  $[-3, 3]$  and 3 coupling layers. The conditioner for the NSF is an MLP with 2 hidden layer of 30 units, and 10% dropout, trained for 400 epochs.

**Evaluations details.** We use the same setting as the g-and-k experiment for NPE except that we use 980 test simulations for evaluation.